

Durham Research Online

Deposited in DRO:

08 April 2019

Version of attached file:

Published Version

Peer-review status of attached file:

Peer-reviewed

Citation for published item:

Toma, Takashi and Vicente, Avelino (2014) 'Lepton flavor violation in the scotogenic model.', Journal of high energy physics., 2014 (1). p. 160.

Further information on publisher's website:

[https://doi.org/10.1007/JHEP01\(2014\)160](https://doi.org/10.1007/JHEP01(2014)160)

Publisher's copyright statement:

This article is distributed under the terms of the Creative Commons Attribution License (CC-BY 4.0), which permits any use, distribution and reproduction in any medium, provided the original author(s) and source are credited.

Additional information:

Use policy

The full-text may be used and/or reproduced, and given to third parties in any format or medium, without prior permission or charge, for personal research or study, educational, or not-for-profit purposes provided that:

- a full bibliographic reference is made to the original source
- a [link](#) is made to the metadata record in DRO
- the full-text is not changed in any way

The full-text must not be sold in any format or medium without the formal permission of the copyright holders.

Please consult the [full DRO policy](#) for further details.

Lepton flavor violation in the scotogenic model

Takashi Toma^a and Avelino Vicente^b

^a*Institute for Particle Physics Phenomenology, University of Durham,
South Road, Durham, DH1 3LE, United Kingdom*

^b*IFPA, Dep. AGO, Université de Liège,
Bat B5, Sart-Tilman B-4000, Liège 1, Belgium*

E-mail: takashi.toma@durham.ac.uk, avelino.vicente@ulg.ac.be

ABSTRACT: We investigate lepton flavor violation in the scotogenic model proposed by Ma in which neutrinos acquire non-zero masses at the 1-loop level. Although some works exist in this direction, they have mainly focused on the radiative decay $\ell_\alpha \rightarrow \ell_\beta \gamma$. Motivated by the promising new projects involving other low-energy processes, we derive complete analytical expressions for $\ell_\alpha \rightarrow 3\ell_\beta$ and $\mu - e$ conversion in nuclei, and numerically study their impact on the phenomenology. We will show that these processes can actually have rates larger than the one for $\ell_\alpha \rightarrow \ell_\beta \gamma$, thus providing more stringent constraints and better experimental perspectives.

KEYWORDS: Rare Decays, Neutrino Physics, Beyond Standard Model

ARXIV EPRINT: [1312.2840](https://arxiv.org/abs/1312.2840)

Contents

1	Introduction	1
2	The model	2
3	Analytical results	4
3.1	$\ell_\alpha \rightarrow \ell_\beta \gamma$	4
3.2	$\ell_\alpha \rightarrow 3 \ell_\beta$	5
3.3	$\mu - e$ conversion in nuclei	7
4	Phenomenological discussion	9
4.1	The ratio $\text{Br}(\ell_\alpha \rightarrow 3 \ell_\beta)/\text{Br}(\ell_\alpha \rightarrow \ell_\beta \gamma)$	9
4.2	Sensitivity to low-energy neutrino parameters	15
4.3	$\mu - e$ conversion in nuclei	17
5	Summary and conclusions	19
A	Loop functions	21
B	Flavor structures	22

1 Introduction

The search for lepton flavor violation (LFV) is going to live an unprecedented era with great experimental efforts in many different fronts. In addition to the well-known searches for the radiative decay $\ell_\alpha \rightarrow \ell_\beta \gamma$, new projects involving other low-energy processes, such as $\ell_\alpha \rightarrow 3 \ell_\beta$ or $\mu - e$ conversion in nuclei, are going to look for a positive LFV signal.

For many years, the experiment leading to the most stringent constraints has been MEG [1]. This experiment, which searches for the radiative decay $\mu \rightarrow e \gamma$, recently published a new limit, $\text{Br}(\mu \rightarrow e \gamma) < 5.7 \times 10^{-13}$, obtained with an updated analysis of the 2009-2010 data sample together with the analysis of the new data collected in 2011 [2]. The expectation is that MEG can reduce the current bound by another order of magnitude, with sensitivities of about 6×10^{-14} after 3 years of acquisition time [3].

However, the most impressive improvements in the next few years are expected in $\mu \rightarrow 3e$ and $\mu - e$ conversion in nuclei. For the former, the Mu3e experiment is expected to reach a sensitivity of 10^{-15} (after upgrades 10^{-16}) [4]. This would imply an improvement of 3-4 orders of magnitude with respect to the current bound. For $\mu - e$ conversion in nuclei several project will compete in the next few years. These include Mu2e [5, 6], DeeMe [7], COMET [8] and PRISM/PRIME [9]. The expected sensitivities for the conversion rate range from a modest 10^{-14} to an impressive 10^{-18} .

Finally, the limits for τ observables are less stringent, although significant improvements are expected at B factories [10, 11]. Table 1 summarizes the current experimental bounds and future sensitivities for the low-energy LFV observables.

Different observables may have very different rates for a given model. For example, the rates for $\mu \rightarrow 3e$ and $\mu - e$ conversion in nuclei are typically suppressed with respect to $\mu \rightarrow e\gamma$ in models where the dominant LFV contributions are induced by dipole operators, like the Minimal Supersymmetric Standard Model. However, there are many frameworks where this is not the case. For this reason, one needs to fully understand the *anatomy* of LFV in each model in order to determine the expected hierarchies among observables, which then become indirect tests of the model.

In this paper we pursue this goal in the context of a model proposed by Ma in which neutrinos acquire masses at the 1-loop level [17]. The same symmetry that forbids the tree-level contribution to Dirac neutrino masses, a \mathbb{Z}_2 parity, also gives rise to a dark matter candidate. This simple extension of the Standard Model (SM), usually called *Scotogenic Model*, constitutes a very simple framework to address the most important motivations to go beyond.¹ Although some works have been already done regarding LFV in this model [29–32], they have either focused on $\mu \rightarrow e\gamma$ or neglected contributions beyond the photonic dipole. To the best of our knowledge, this is the first time $\ell_\alpha \rightarrow 3\ell_\beta$ and $\mu - e$ conversion in nuclei are fully considered. As we will see, these processes might actually have rates larger than the one for $\mu \rightarrow e\gamma$, thus providing better bounds and experimental perspectives.

The rest of the paper is organized as follows: in section 2 we describe the model and its basic features. In section 3 we present our analytical results, whereas section 4 contains a numerical discussion addressing some phenomenological issues of interest. Finally, we summarize our results and conclude in section 5.

2 The model

The model under consideration [17] adds three right-handed neutrinos N_i ($i = 1-3$) and one $SU(2)_L$ doublet η to the SM particle content. In addition, a \mathbb{Z}_2 parity is imposed, under which the new particles are odd and the SM ones are even.² The interaction of the right-handed neutrino sector is described by the Lagrangian

$$\mathcal{L}_N = \overline{N}_i \not{\partial} N_i - \frac{m_{N_i}}{2} \overline{N}_i^c P_R N_i + y_{i\alpha} \eta \overline{N}_i P_L \ell_\alpha + \text{h.c.} \quad (2.1)$$

Note that one can always write the right-handed neutrino mass term as a diagonal matrix without loss of generality. The scalar potential \mathcal{V} is given by

$$\begin{aligned} \mathcal{V} = & m_\phi^2 \phi^\dagger \phi + m_\eta^2 \eta^\dagger \eta + \frac{\lambda_1}{2} (\phi^\dagger \phi)^2 + \frac{\lambda_2}{2} (\eta^\dagger \eta)^2 + \lambda_3 (\phi^\dagger \phi) (\eta^\dagger \eta) \\ & + \lambda_4 (\phi^\dagger \eta) (\eta^\dagger \phi) + \frac{\lambda_5}{2} \left[(\phi^\dagger \eta)^2 + (\eta^\dagger \phi)^2 \right]. \end{aligned} \quad (2.2)$$

¹For other recent works on further extended models with radiative neutrino masses, see for example [18–28].

²Due to the conservation of the \mathbb{Z}_2 symmetry, the left-handed neutrinos in the SM lepton doublet do not form a Dirac pair with the ‘right-handed’ neutrinos N_i . For this reason, strictly speaking, it is not correct to call the N_i singlets right-handed neutrinos. Nevertheless, this has become common practice in the literature and we will stick to this denomination.

LFV Process	Present Bound	Future Sensitivity
$\mu \rightarrow e\gamma$	5.7×10^{-13} [2]	6×10^{-14} [3]
$\tau \rightarrow e\gamma$	3.3×10^{-8} [12]	$\sim 10^{-8} - 10^{-9}$ [11]
$\tau \rightarrow \mu\gamma$	4.4×10^{-8} [12]	$\sim 10^{-8} - 10^{-9}$ [11]
$\mu \rightarrow 3e$	1.0×10^{-12} [13]	$\sim 10^{-16}$ [4]
$\tau \rightarrow 3e$	2.7×10^{-8} [14]	$\sim 10^{-9} - 10^{-10}$ [11]
$\tau \rightarrow 3\mu$	2.1×10^{-8} [14]	$\sim 10^{-9} - 10^{-10}$ [11]
$\mu^-, \text{Au} \rightarrow e^-, \text{Au}$	7.0×10^{-13} [15]	—
$\mu^-, \text{Ti} \rightarrow e^-, \text{Ti}$	4.3×10^{-12} [16]	$\sim 10^{-18}$ [9]

Table 1. Current experimental bounds and future sensitivities for some low-energy LFV observables.

We assume that the parameters in the scalar potential are such that the doublet η does not get a vacuum expectation value. This is fundamental in order to keep the \mathbb{Z}_2 symmetry unbroken. After electroweak symmetry breaking, the masses of the charged component η^+ and neutral component $\eta^0 = (\eta_R + i\eta_I)/\sqrt{2}$ are split to

$$m_{\eta^+}^2 = m_\eta^2 + \lambda_3 \langle \phi^0 \rangle^2 \quad (2.3)$$

$$m_R^2 = m_\eta^2 + (\lambda_3 + \lambda_4 + \lambda_5) \langle \phi^0 \rangle^2, \quad (2.4)$$

$$m_I^2 = m_\eta^2 + (\lambda_3 + \lambda_4 - \lambda_5) \langle \phi^0 \rangle^2, \quad (2.5)$$

where the mass difference between η_R and η_I is $m_R^2 - m_I^2 = 2\lambda_5 \langle \phi^0 \rangle^2$.

After symmetry breaking, the light neutrino masses are generated at the 1-loop level.³ The neutrino mass matrix can be expressed as

$$\begin{aligned} (m_\nu)_{\alpha\beta} &= \sum_{i=1}^3 \frac{y_{i\alpha} y_{i\beta}}{(4\pi)^2} m_{N_i} \left[\frac{m_R^2}{m_R^2 - m_{N_i}^2} \log \left(\frac{m_R^2}{m_{N_i}^2} \right) - \frac{m_I^2}{m_I^2 - m_{N_i}^2} \log \left(\frac{m_I^2}{m_{N_i}^2} \right) \right] \\ &\equiv (y^T \Lambda y)_{\alpha\beta}, \end{aligned} \quad (2.6)$$

where m_R and m_I are the masses of η_R and η_I respectively, and the Λ matrix is defined as

$$\Lambda = \begin{pmatrix} \Lambda_1 & 0 & 0 \\ 0 & \Lambda_2 & 0 \\ 0 & 0 & \Lambda_3 \end{pmatrix}, \quad \Lambda_i = \frac{m_{N_i}}{(4\pi)^2} \left[\frac{m_R^2}{m_R^2 - m_{N_i}^2} \log \left(\frac{m_R^2}{m_{N_i}^2} \right) - \frac{m_I^2}{m_I^2 - m_{N_i}^2} \log \left(\frac{m_I^2}{m_{N_i}^2} \right) \right]. \quad (2.7)$$

In particular, when $m_R^2 \approx m_I^2 \equiv m_0^2$ ($\lambda_5 \ll 1$), the mass matrix gets the simplified form

$$(m_\nu)_{\alpha\beta} \approx \sum_{i=1}^3 \frac{2\lambda_5 y_{i\alpha} y_{i\beta} \langle \phi^0 \rangle^2}{(4\pi)^2 m_{N_i}} \left[\frac{m_{N_i}^2}{m_0^2 - m_{N_i}^2} + \frac{m_{N_i}^4}{(m_0^2 - m_{N_i}^2)^2} \log \left(\frac{m_{N_i}^2}{m_0^2} \right) \right]. \quad (2.8)$$

³Note that the tree-level contribution is actually forbidden by the \mathbb{Z}_2 discrete symmetry.

This neutrino mass matrix is diagonalized as

$$U_{\text{PMNS}}^T m_\nu U_{\text{PMNS}} = \hat{m}_\nu \equiv \begin{pmatrix} m_1 & 0 & 0 \\ 0 & m_2 & 0 \\ 0 & 0 & m_3 \end{pmatrix}, \quad (2.9)$$

where

$$U_{\text{PMNS}} = \begin{pmatrix} c_{12}c_{13} & s_{12}c_{13} & s_{13}e^{i\delta} \\ -s_{12}c_{23} - c_{12}s_{23}s_{13}e^{-i\delta} & c_{12}c_{23} - s_{12}s_{23}s_{13}e^{-i\delta} & s_{23}c_{13} \\ s_{12}s_{23} - c_{12}c_{23}s_{13}e^{-i\delta} & -c_{12}s_{23} - s_{12}c_{23}s_{13}e^{-i\delta} & c_{23}c_{13} \end{pmatrix} \times \begin{pmatrix} e^{i\varphi_1/2} & 0 & 0 \\ 0 & e^{i\varphi_2/2} & 0 \\ 0 & 0 & 1 \end{pmatrix} \quad (2.10)$$

is the PMNS (Pontecorvo-Maki-Nakagawa-Sakata) matrix. Here $c_{ij} = \cos \theta_{ij}$, $s_{ij} = \sin \theta_{ij}$, δ is the Dirac phase and φ_1, φ_2 are the Majorana phases.⁴

The Yukawa matrix $y_{i\alpha}$ can be written using an adapted Casas-Ibarra parametrization [33] as

$$y = \sqrt{\Lambda}^{-1} R \sqrt{\hat{m}_\nu} U_{\text{PMNS}}^\dagger, \quad (2.11)$$

where R is a complex orthogonal matrix which satisfies $R^T R = 1$.

3 Analytical results

In this section we present our analytical results for the LFV processes $\ell_\alpha \rightarrow \ell_\beta \gamma$, $\ell_\alpha \rightarrow 3 \ell_\beta$ and $\mu - e$ conversion in nuclei. Before we proceed to the analytical discussion a comment is in order. It is well-known that the rates for LFV processes get greatly enhanced in models with right-handed neutrinos at the electroweak scale [34–42]. This is due to the fact that the GIM suppression at work in the SM contribution is spoiled by the mixing between left- and right-handed neutrinos. One could naively think that this is also the case in the scotogenic model. However, the unbroken \mathbb{Z}_2 symmetry forbids this mixing, (see footnote 2), and thus the enhancement in the $W - \nu$ loops is not present. We will show that the enhancement is still possible, but with $\eta^\pm - N$ loops instead.

3.1 $\ell_\alpha \rightarrow \ell_\beta \gamma$

The most popular searches for LFV have focused on the radiative process $\ell_\alpha \rightarrow \ell_\beta \gamma$. This is described by the effective Lagrangian

$$\mathcal{L}_{\text{eff}} = \left(\frac{\mu_{\beta\alpha}}{2} \right) \bar{\ell}_\beta \sigma^{\mu\nu} \ell_\alpha F_{\mu\nu}, \quad (3.1)$$

where $\mu_{\beta\alpha}$ is a transition magnetic moment. It proves convenient to define it in terms of the dipole form factor A_D as $\mu_{\beta\alpha} = e m_\alpha A_D / 2$, where terms proportional to m_β have been neglected and e is the electromagnetic coupling, related to the electromagnetic fine structure constant as $\alpha_{\text{em}} = e^2 / (4\pi)$. In the model under consideration, A_D gets contributions

⁴We will neglect Majorana phases in all our computations.

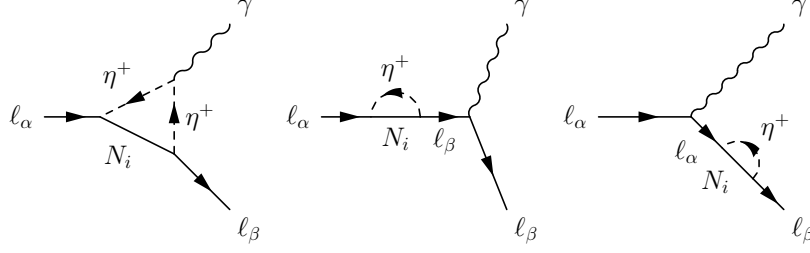


Figure 1. 1-loop Feynman diagrams leading to $\ell_\alpha \rightarrow \ell_\beta \gamma$.

at the 1-loop level from the Feynman diagrams in figure 1. They lead to the following expression

$$A_D = \sum_{i=1}^3 \frac{y_{i\beta}^* y_{i\alpha}}{2(4\pi)^2 m_{\eta^+}^2} F_2(\xi_i), \quad (3.2)$$

where the ξ_i parameters are defined as $\xi_i \equiv m_{N_i}^2/m_{\eta^+}^2$ and the loop function $F_2(x)$ is given in appendix A. Finally, the branching fraction for $\ell_\alpha \rightarrow \ell_\beta \gamma$ is calculated as

$$\text{Br}(\ell_\alpha \rightarrow \ell_\beta \gamma) = \frac{3(4\pi)^3 \alpha_{\text{em}}}{4G_F^2} |A_D|^2 \text{Br}(\ell_\alpha \rightarrow \ell_\beta \nu_\alpha \bar{\nu}_\beta), \quad (3.3)$$

where G_F is the Fermi constant.

3.2 $\ell_\alpha \rightarrow 3 \ell_\beta$

Next we consider the process $\ell_\alpha \rightarrow 3 \ell_\beta$ (more precisely denoted as $\ell_\alpha \rightarrow \ell_\beta \bar{\ell}_\beta \ell_\beta$). Although this has attracted less attention, important projects are going to be launched in the near future, with the Mu3e experiment as the leading one. There are four types of 1-loop diagrams that contribute to $\ell_\alpha \rightarrow 3 \ell_\beta$. These are γ -penguins, Z -penguins, Higgs-penguins and box diagrams. In our computations we did not consider Higgs-penguins, since we are mostly interested in processes involving the first two charged lepton generations, whose small Yukawa couplings suppress Higgs contributions. Notice that this assumption would not be valid for LFV processes involving τ leptons. However, the experimental limits in this case are not as stringent as those found for processes involving the first two generations, and thus their consideration would not change the phenomenological picture.

Let us consider the momentum assignment $\ell_\alpha(p) \rightarrow \ell_\beta(k_1) \bar{\ell}_\beta(k_2) \ell_\beta(k_3)$. Then, the γ -penguin diagrams shown in figure 2 lead to the amplitude⁵

$$\begin{aligned} i\mathcal{M}_\gamma = & ie^2 A_{ND} \bar{u}(k_1) \gamma^\mu P_L u(p) \bar{u}(k_3) \gamma_\mu v(k_2) \\ & + ie^2 \frac{m_\alpha}{q^2} A_D \bar{u}(k_1) \sigma^{\mu\nu} q_\nu P_R u(p) \bar{u}(k_3) \gamma_\mu v(k_2) - (k_1 \leftrightarrow k_3), \end{aligned} \quad (3.4)$$

where $q \equiv k_1 - p$ is the photon momentum. Other operators turn out to be suppressed by charged lepton masses and thus they are neglected in eq. (3.4). The coefficient A_D

⁵In the presentation of our results we will follow a notation inspired by [43], which improved on [44].

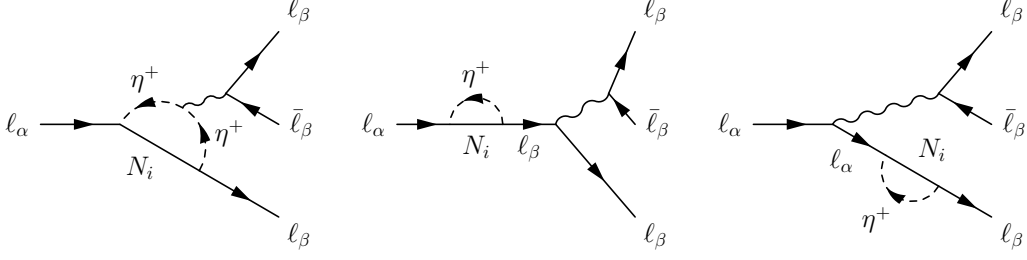


Figure 2. Penguin contributions to $\ell_\alpha \rightarrow 3\ell_\beta$. The wavy line represents either a photon or a Z-boson.

was given in eq. (3.2), whereas the coefficient A_{ND} , which corresponds to the photonic non-dipole contributions, is given by

$$A_{ND} = \sum_{i=1}^3 \frac{y_{i\beta}^* y_{i\alpha}}{6(4\pi)^2} \frac{1}{m_{\eta^+}^2} G_2(\xi_i), \quad (3.5)$$

where the loop function $G_2(x)$ is given in appendix A.

Similarly, we now consider the contributions from Z-penguin diagrams, also shown in figure 2. Neglecting sub-dominant terms proportional to q^2 , q being the 4-momentum of the Z-boson, the resulting amplitude can be written as

$$i\mathcal{M}_Z = \frac{iF}{m_Z^2} \bar{u}(k_1)\gamma^\mu P_R u(p)\bar{u}(k_3)\gamma_\mu \left(g_L^\ell P_L + g_R^\ell P_R\right) v(k_2) - (k_1 \leftrightarrow k_3), \quad (3.6)$$

where

$$g_L^\ell = \frac{g_2}{\cos\theta_W} \left(\frac{1}{2} - \sin^2\theta_W\right), \quad g_R^\ell = -\frac{g_2}{\cos\theta_W} \sin^2\theta_W, \quad (3.7)$$

are the tree-level Z-boson couplings to a pair of charged leptons. Here g_2 is the $SU(2)_L$ gauge coupling and θ_W is the weak mixing angle. The coefficient F is given by

$$F = \sum_{i=1}^3 \frac{y_{i\beta}^* y_{i\alpha}}{2(4\pi)^2} \frac{m_\alpha m_\beta}{m_{\eta^+}^2} \frac{g_2}{\cos\theta_W} F_2(\xi_i). \quad (3.8)$$

Equation (3.8) shows that Z-penguins are suppressed by the charged lepton masses m_α and m_β . Therefore, although we fully derived and included them in our computation, we found that they always have negligible contributions to the LFV processes considered in this paper. For this reason, the total decay width for $\ell_\alpha \rightarrow 3\ell_\beta$ will be mainly given by the γ -penguins and the box contributions, whose relative size will determine the phenomenology.

Finally, the box diagrams contributing to the process $\ell_\alpha \rightarrow 3\ell_\beta$ are shown in figure 3. One finds the following amplitude

$$i\mathcal{M}_{\text{box}} = ie^2 B [\bar{u}(k_3)\gamma^\mu P_L v(k_2)] [\bar{u}(k_1)\gamma_\mu P_L u(p)]. \quad (3.9)$$

The coefficient B is given by⁶

$$e^2 B = \frac{1}{(4\pi)^2 m_{\eta^+}^2} \sum_{i,j=1}^3 \left[\frac{1}{2} D_1(\xi_i, \xi_j) y_{j\beta}^* y_{j\beta} y_{i\beta}^* y_{i\alpha} + \sqrt{\xi_i \xi_j} D_2(\xi_i, \xi_j) y_{j\beta}^* y_{j\beta} y_{i\beta}^* y_{i\alpha} \right], \quad (3.10)$$

⁶In [43] this coefficient was denoted as B_1^L . The rest of box contributions are clearly suppressed in the scotogenic model.

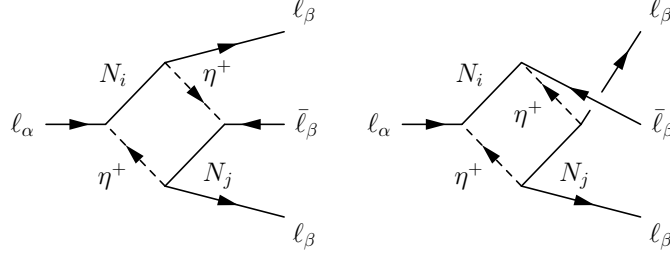


Figure 3. Box contributions to $\ell_\alpha \rightarrow 3 \ell_\beta$.

where the loop functions $D_1(x, y)$ and $D_2(x, y)$ are given in appendix A. The branching ratio for $\ell_\alpha \rightarrow 3 \ell_\beta$ is given by

$$\begin{aligned} \text{Br}(\ell_\alpha \rightarrow \ell_\beta \bar{\ell}_\beta \ell_\beta) &= \frac{3(4\pi)^2 \alpha_{\text{em}}^2}{8G_F^2} \left[|A_{ND}|^2 + |A_D|^2 \left(\frac{16}{3} \log \left(\frac{m_\alpha}{m_\beta} \right) - \frac{22}{3} \right) + \frac{1}{6} |B|^2 \right. \\ &\quad \left. + \frac{1}{3} (2|F_{RR}|^2 + |F_{RL}|^2) + \left(-2A_{ND}A_D^* + \frac{1}{3}A_{ND}B^* - \frac{2}{3}A_DB^* + \text{h.c.} \right) \right] \\ &\quad \times \text{Br}(\ell_\alpha \rightarrow \ell_\beta \nu_\alpha \bar{\nu}_\beta), \end{aligned} \quad (3.11)$$

where F_{RR} and F_{RL} are given by

$$F_{RR} = \frac{F g_R^\ell}{g_2^2 \sin^2 \theta_W m_Z^2}, \quad F_{RL} = \frac{F g_L^\ell}{g_2^2 \sin^2 \theta_W m_Z^2}. \quad (3.12)$$

In eq. (3.11), the mass of the charged lepton in the final state, m_β , is kept only in the logarithmic term, where it plays the role of regulating the infrared divergence that would appear otherwise.

3.3 $\mu - e$ conversion in nuclei

The most remarkable experimental projects in the near future will be devoted to searches for $\mu - e$ conversion in nuclei. The great sensitivities announced by the different collaborations might make this observable the most stringent one in most neutrino mass models. We will present our results using the notation and conventions of refs. [45, 46]. The conversion rate, relative to the muon capture rate, can be expressed as

$$\begin{aligned} \text{CR}(\mu - e, \text{Nucleus}) &= \frac{p_e E_e m_\mu^3 G_F^2 \alpha_{\text{em}}^3 Z_{\text{eff}}^4 F_p^2}{8 \pi^2 Z} \\ &\quad \times \left\{ \left| (Z + N) \left(g_{LV}^{(0)} + g_{LS}^{(0)} \right) + (Z - N) \left(g_{LV}^{(1)} + g_{LS}^{(1)} \right) \right|^2 + \right. \\ &\quad \left. \left| (Z + N) \left(g_{RV}^{(0)} + g_{RS}^{(0)} \right) + (Z - N) \left(g_{RV}^{(1)} + g_{RS}^{(1)} \right) \right|^2 \right\} \frac{1}{\Gamma_{\text{capt}}}. \end{aligned} \quad (3.13)$$

Here Z and N are the number of protons and neutrons in the nucleus, Z_{eff} is the effective atomic charge (see [47]), F_p is the nuclear matrix element and Γ_{capt} represents the total muon capture rate. The values of these parameters for the nuclei used in experiments can be found in [46] and references therein. Furthermore, p_e and E_e (taken to be $\simeq m_\mu$ in the

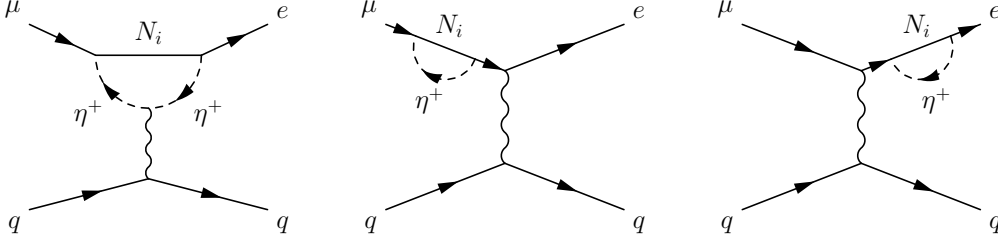


Figure 4. Penguin contributions to $\mu - e$ conversion in nuclei. The wavy line represents either a photon or a Z -boson.

numerical evaluation) are the momentum and energy of the electron and m_μ is the muon mass. In the above, $g_{XK}^{(0)}$ and $g_{XK}^{(1)}$ (with $X = L, R$ and $K = S, V$) are given by

$$\begin{aligned} g_{XK}^{(0)} &= \frac{1}{2} \sum_{q=u,d,s} \left(g_{XK(q)} G_K^{(q,p)} + g_{XK(q)} G_K^{(q,n)} \right), \\ g_{XK}^{(1)} &= \frac{1}{2} \sum_{q=u,d,s} \left(g_{XK(q)} G_K^{(q,p)} - g_{XK(q)} G_K^{(q,n)} \right). \end{aligned} \quad (3.14)$$

The numerical values of the G_K coefficients can be found in [45, 46, 48].

As for $\ell_\alpha \rightarrow 3\ell_\beta$, the $\mu - e$ conversion rate receives contributions from γ -, Z - and Higgs-penguins. Note, however, the absence of box contributions (besides the tiny SM contribution). This is due to the unbroken \mathbb{Z}_2 symmetry, which forbids the coupling between the η^\pm scalars and the quark sector. Moreover, we neglect again the Higgs-penguin contributions due to the smallness of the involved Yukawa couplings. Therefore, the corresponding couplings are

$$\begin{aligned} g_{LV(q)} &= g_{LV(q)}^\gamma + g_{LV(q)}^Z, \\ g_{RV(q)} &= g_{LV(q)} \Big|_{L \leftrightarrow R}, \\ g_{LS(q)} &\approx 0, \\ g_{RS(q)} &\approx 0. \end{aligned} \quad (3.15)$$

The photon and Z -boson couplings can be computed from the Feynman diagrams in figure 4. One finds that the relevant (non-negligible) couplings are

$$\begin{aligned} g_{LV(q)}^\gamma &= \frac{\sqrt{2}}{G_F} e^2 Q_q (A_{ND} - A_D), \\ g_{RV(q)}^Z &= -\frac{\sqrt{2}}{G_F} \frac{g_L^q + g_R^q}{2} \frac{F}{m_Z^2}. \end{aligned} \quad (3.16)$$

The form factors A_{ND} , A_D and F are given in section 3.2, see equations (3.5), (3.2) and (3.8). Furthermore, Q_q is the electric charge of the corresponding quark and

$$g_L^q = \frac{g_2}{\cos \theta_W} (Q_q \sin^2 \theta_W - T_3^q), \quad g_R^q = \frac{g_2}{\cos \theta_W} Q_q \sin^2 \theta_W, \quad (3.17)$$

are the tree-level Z -boson couplings to a pair of quarks.

4 Phenomenological discussion

In this section we present and discuss our numerical results. We will explore the parameter space and highlight some relevant phenomenological issues which, to the best of our knowledge, have not been discussed in the existing literature.

In the numerical evaluation of our results we considered both hierarchies for the light neutrino spectrum,⁷ normal hierarchy (NH) and inverted hierarchy (IH), and randomly chose the neutrino oscillation parameters in the 1σ ranges found by the global fit [49] (*Free Fluxes + RSBL* results). We note that these ranges are in good agreement with the ones found by other fits, see refs. [50, 51]. For θ_{23} , the atmospheric angle, we selected the local minimum in the first octant, in agreement with [51].

Unless explicitly expressed otherwise, all our numerical results were obtained for a degenerate right-handed neutrino spectrum, assuming a random real R matrix and $\lambda_5 = 10^{-9}$. This value was found in [52] to be compatible with a correct right-handed neutrino DM relic density due to the resulting size of the Yukawa couplings. Moreover, note that it is natural for λ_5 to be very small since, in case it was exactly zero, a definition of a conserved lepton number would be possible [29].

4.1 The ratio $\text{Br}(\ell_\alpha \rightarrow 3\ell_\beta)/\text{Br}(\ell_\alpha \rightarrow \ell_\beta\gamma)$

Most LFV phenomenological studies focus on the radiative decay $\mu \rightarrow e\gamma$, ignoring other LFV observables. There are two reasons for this. First, the great performance of the MEG experiment, that recently set the quite impressive bound $\text{Br}(\mu \rightarrow e\gamma) < 5.7 \times 10^{-13}$. And second, the dipole dominance in many models of interest. When the dipole contributions originated in photon penguin diagrams dominate, the rate for $\mu \rightarrow 3e$ is correlated with the rate for $\mu \rightarrow e\gamma$. In this case a simple relation can be derived [43]

$$\text{Br}(\mu \rightarrow 3e) \simeq \frac{\alpha_{\text{em}}}{3\pi} \left(\log \left(\frac{m_\mu^2}{m_e^2} \right) - \frac{11}{4} \right) \text{Br}(\mu \rightarrow e\gamma). \quad (4.1)$$

Since the proportionality factor is much smaller than one, $\mu \rightarrow 3e$ is suppressed with respect to $\mu \rightarrow e\gamma$ and the latter becomes the process leading to the most stringent constraints. This assumption has been present in all previous works on lepton flavor violation in the scotogenic model [29–32]. They have either assumed explicitly that photon penguin diagrams dominate or simply ignored 4-fermion observables (like $\mu \rightarrow 3e$) and concentrated on $\mu \rightarrow e\gamma$ (an approach consistent with the assumption that the photonic dipole contributions dominate). Here we want to study under what conditions that is a bad simplification of the phenomenology. In order to do so, we consider the ratio⁸

$$R_{\mu e} = \frac{\text{Br}(\mu \rightarrow 3e)}{\text{Br}(\mu \rightarrow e\gamma)}. \quad (4.2)$$

⁷In our conventions, the lightest neutrino mass is m_1 for normal hierarchy and m_3 for inverted hierarchy, although we will denote it by m_{ν_1} in general.

⁸We concentrate here on μ decays due to the better experimental bounds and perspectives. Similar results are obtained for τ decays.

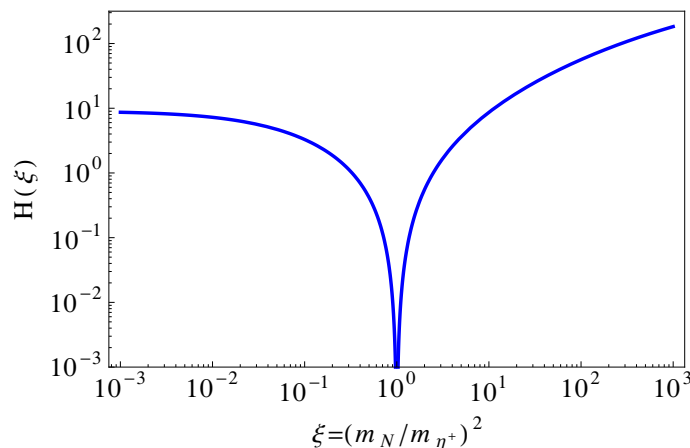


Figure 5. $H(\xi)$ as a function of $\xi = (m_N/m_{\eta^+})^2$. For the definition see eq. (4.4).

In those regions of parameter space where $R_{\mu e} > 1$, the observable that provides the most stringent limits is $\text{Br}(\mu \rightarrow 3e)$, whereas $\text{Br}(\mu \rightarrow e\gamma)$ would be the most relevant observable in regions where $R_{\mu e} < 1$.

Since the photonic dipole operators contribute to both observables, the only way to obtain $R_{\mu e} > 1$ is to have dominant contributions from box and/or photonic non-dipole diagrams in $\mu \rightarrow 3e$ (Z -penguins are suppressed by charged leptons and thus their contribution is always negligible). Since the photonic non-dipole diagrams, given by the A_{ND} form factor, never exceed the dipole ones as much as to compensate the large factor that multiplies $|A_D|^2$ in the branching ratio formula (see eq. (3.11)), they are never dominant. We are therefore left with a *competition* between photonic dipole operators and box diagrams.

Assuming box dominance in $\mu \rightarrow 3e$ and a degenerate right-handed neutrino spectrum one can estimate

$$R_{\mu e} \sim \frac{y^4}{48\pi^2 e^2} H(\xi), \quad (4.3)$$

where y is the average size of the Yukawa coupling and the function $H(\xi)$ is defined as

$$H(\xi) = \left(\frac{\frac{1}{2}D_1(\xi, \xi) + \xi D_2(\xi, \xi)}{F_2(\xi)} \right)^2. \quad (4.4)$$

The function $H(\xi)$ is shown in figure 5. Notice the cancellation for $\xi = 1$. This pole is caused by an exact cancellation between the contributions from the loop functions D_1 and D_2 . However, for $\xi \ll 1$ and $\xi \gg 1$ one always has $H(\xi) > 1$.

It is clear from eq. (4.3) and figure 5 that in order to increase the value of $R_{\mu e}$ one requires large Yukawa couplings and a large mass difference between the right-handed neutrinos and the η scalars (in order to be far from $\xi = 1$). This is illustrated in figure 6, where we show $\text{Br}(\mu \rightarrow e\gamma)$ (blue) and $\text{Br}(\mu \rightarrow 3e)$ (red) as a function of $\xi = (m_N/m_{\eta^+})^2$. The horizontal dashed lines represent the current upper bounds on the branching ratios. Fixed values $m_{\eta^+} = 1 \text{ TeV}$ and $m_{\nu_1} = 10^{-3} \text{ eV}$ (lightest neutrino mass) are taken. On the left-hand side we show our results for NH, whereas the right-hand side shows our results

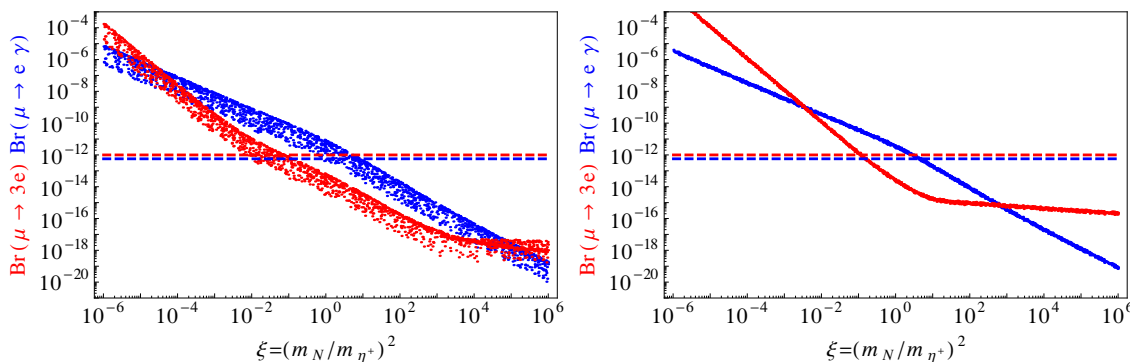


Figure 6. $\text{Br}(\mu \rightarrow e\gamma)$ and $\text{Br}(\mu \rightarrow 3e)$ as a function of $\xi = (m_N/m_{\eta^+})^2$. A degenerate right-handed neutrino spectrum has been assumed, see text for details. To the left for NH, whereas to the right for IH. The horizontal dashed lines show the current upper bounds.

for IH. A random Dirac phase δ has been taken. As can be derived from the spread of the points, this parameter has a much larger influence for NH. As expected from our previous estimate, one can in principle have $R_{\mu e} > 1$ (or equivalently, $\text{Br}(\mu \rightarrow 3e) > \text{Br}(\mu \rightarrow e\gamma)$) for ξ values far from 1. Although the region with $m_N \ll m_{\eta^+}$ is already excluded for this value of λ_5 , the region with $m_N \gg m_{\eta^+}$ is compatible with all experimental constraints. Note that in this figure all points have $\mathcal{O}(1)$ Yukawa couplings. Larger values for λ_5 would decrease the size of the Yukawa couplings (see eq. (2.6)), which in turn would imply a reduction of all LFV rates.

Another parameter that turns out to be very relevant in the determination of the ratio $R_{\mu e}$ is m_{ν_1} , the mass of the lightest neutrino. In order to illustrate this fact, we consider two scenarios: (i) Scenario A: $m_N = 1$ TeV and $m_{\eta^+} = 4$ TeV, and (ii) Scenario B: $m_N = 4$ TeV and $m_{\eta^+} = 1$ TeV. In both cases we assume a degenerate right-handed neutrino spectrum, a random Dirac phase and a random real R matrix.

Our numerical results for scenario A are shown in figures 7 and 8. The left-hand side of these figures were obtained with NH, whereas the right-hand side shows our results for IH. We see that large values of the lightest neutrino mass may lead to large variations in the $\text{Br}(\mu \rightarrow e\gamma)$ and $\text{Br}(\mu \rightarrow 3e)$ branching ratios, and thus in the ratio $R_{\mu e}$. We conclude that the LFV rates in the scotogenic model are very sensitive to the absolute scale for neutrino masses.

Figure 7 demonstrates that in scenario A the neutrino mass hierarchy also has a clear impact on the LFV rates. While for low m_{ν_1} , $\text{Br}(\mu \rightarrow 3e)$ is clearly below the upper bound for NH, it is largely excluded for IH since it exceeds it. Similarly, while for low m_{ν_1} the ratio $R_{\mu e}$ is $\sim 10^{-2}$ in NH (as expected from dipole domination), the contributions from box diagrams already lead to a small increase for IH, where $R_{\mu e} \sim 0.5$.

These figures can be understood by analyzing how the Yukawa couplings depend on m_{ν_1} . In particular, we must study the combinations of Yukawa couplings that contribute to the LFV processes considered here. Let us suppose that box diagrams dominate $\ell_\alpha \rightarrow 3\ell_\beta$ (otherwise we would be in a dipole dominated scenario where the ratio $R_{\mu e}$ would not

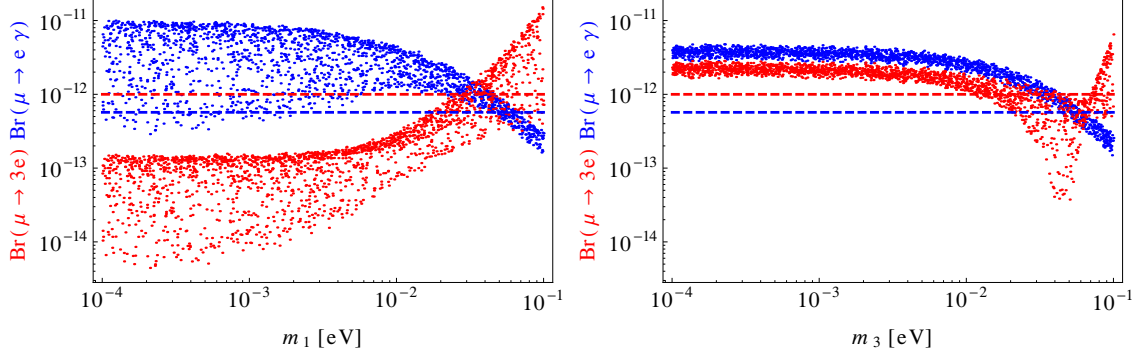


Figure 7. $\text{Br}(\mu \rightarrow e\gamma)$ and $\text{Br}(\mu \rightarrow 3e)$ as a function of the lightest neutrino mass. Scenario A is assumed, see text for details. To the left for NH, whereas to the right for IH. The horizontal dashed lines show the current upper bounds.

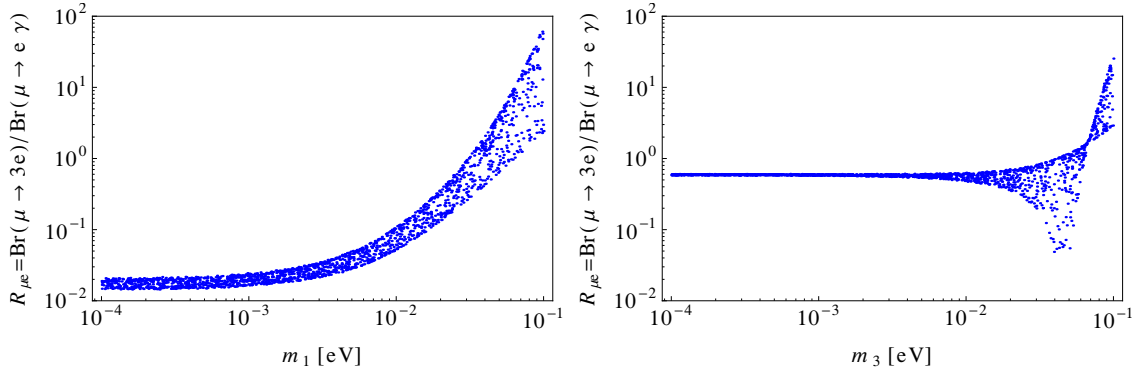


Figure 8. The ratio $R_{\mu e} = \text{Br}(\mu \rightarrow 3e)/\text{Br}(\mu \rightarrow e\gamma)$ as a function of the lightest neutrino mass. Scenario A is assumed, see text for details. To the left for NH, whereas to the right for IH.

deviate significantly from $\sim 10^{-2}$). Then we have the relations

$$\text{Br}(\ell_\alpha \rightarrow \ell_\beta \gamma) \propto \left| (y^\dagger y)_{\beta\alpha} \right|^2 \quad (4.5)$$

$$\text{Br}(\ell_\alpha \rightarrow 3\ell_\beta) \propto \left| \frac{1}{2} D_1(\xi, \xi) (y^\dagger y)_{\beta\beta} (y^\dagger y)_{\beta\alpha} + \xi D_2(\xi, \xi) (y^T y)_{\beta\beta} (y^T y)_{\beta\alpha} \right|^2. \quad (4.6)$$

Assuming degenerate right-handed neutrinos and a real R matrix, we can use the Casas-Ibarra parametrization in eq. (2.11) to obtain

$$y^\dagger y \propto U_{\text{PMNS}} \hat{m}_\nu U_{\text{PMNS}}^\dagger \quad (4.7)$$

$$y^T y \propto U_{\text{PMNS}}^* \hat{m}_\nu U_{\text{PMNS}}^\dagger. \quad (4.8)$$

Analytical results for the relevant elements of the matrix combinations (or *flavor structures*) in the previous expressions can be found in appendix B.

Let us first focus on the NH case. Notice that in scenario A we have $\xi = (1/4)^2 = 0.0625$. With such a small value for ξ , we expect the D_1 term in the box contribution to dominate over the D_2 term. Therefore, we must inspect the expressions for $(y^\dagger y)_{21}$ and

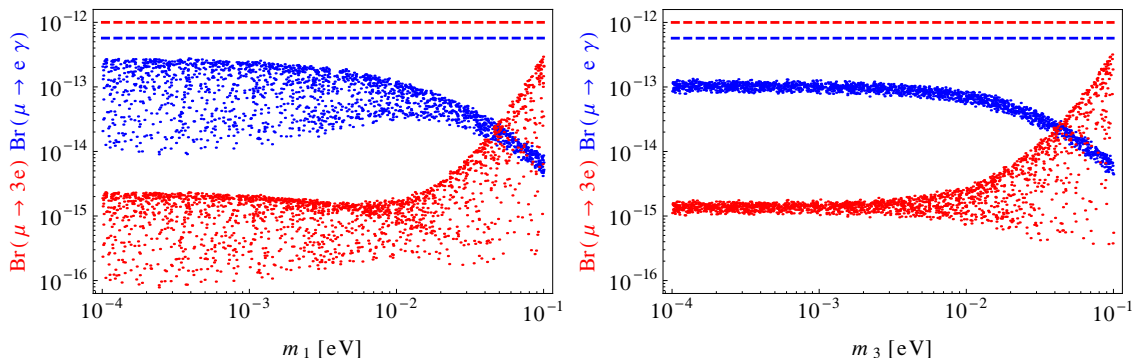


Figure 9. $\text{Br}(\mu \rightarrow e\gamma)$ and $\text{Br}(\mu \rightarrow 3e)$ as a function of the lightest neutrino mass. Scenario B is assumed, see text for details. To the left for NH, whereas to the right for IH. The horizontal dashed lines show the current upper bounds.

$(y^\dagger y)_{22}$ or, as shown above, $(U_{\text{PMNS}} \hat{m}_\nu U_{\text{PMNS}}^\dagger)_{21}$ and $(U_{\text{PMNS}} \hat{m}_\nu U_{\text{PMNS}}^\dagger)_{22}$. On the one hand, we see that $(U_{\text{PMNS}} \hat{m}_\nu U_{\text{PMNS}}^\dagger)_{21}$ depends only on differences of mass eigenvalues. Therefore, it decreases for higher values of the lightest neutrino mass. This can be easily understood from the expansion $m_j - m_i = \Delta m_{ji}^2 / (2m_i) + \dots$, where $\Delta m_{ji}^2 = m_j^2 - m_i^2$ is the corresponding squared mass difference. This expansion is valid for $\Delta m_{ji}^2 / m_i^2 \ll 1$. On the other hand, eq. (B.2) clearly shows that $(U_{\text{PMNS}} \hat{m}_\nu U_{\text{PMNS}}^\dagger)_{22}$ increases for higher values of the lightest neutrino mass. This explains why $\text{Br}(\mu \rightarrow e\gamma)$ decreases with m_{ν_1} while $\text{Br}(\mu \rightarrow 3e)$ increases. The resulting behavior for the ratio $R_{\mu e}$ is then trivially deduced from these considerations. Notice that this quantity can reach values as high as ~ 50 . In this case it is obvious that one cannot ignore $\text{Br}(\mu \rightarrow 3e)$, but in fact this branching ratio becomes the most relevant LFV observable.

The discussion for IH would be a bit more involved. In this case we find a larger relevance of the D_2 piece. In fact, for $m_{\nu_1} \sim 10^{-2}$ eV this term competes with the D_1 term, leading to the feature observed on the right-hand sides of figures 7 and 8.

Let us now consider our results for scenario B, shown in figures 9 and 10. Again, we present our results for NH on the left-hand side and our results for IH on the right-hand side. Regarding NH, it is already clear at first sight that the results are qualitatively very similar to those found in scenario A. Although the LFV rates are very different (much lower in this case), the dependence on m_{ν_1} is very similar. Notice that all points in these figures are actually allowed by the current limits. This was expected, since it is well-known that LFV constraints are more easily satisfied in scenarios with $m_N > m_{\eta^+}$ [29]. On the other hand, the difference between NH and IH found in scenario A is not present in scenario B, in which both cases show the same behavior.

Finally, let us briefly discuss a scenario with non-degenerate right-handed neutrinos. The spectrum in the right-handed neutrino sector has an impact on the LFV rates, as we want to illustrate here. In order to do so, we consider a spectrum of the type $m_N = (\tilde{m}_N, \bar{m}_N^{(1)}, \bar{m}_N^{(2)})$, with two fixed mass eigenvalues $(\bar{m}_N^{(1,2)})$ and one varying (\tilde{m}_N). Although one can imagine other scenarios, this simple family of non-degenerate spectra serves to show the qualitative behavior that we want to emphasize.

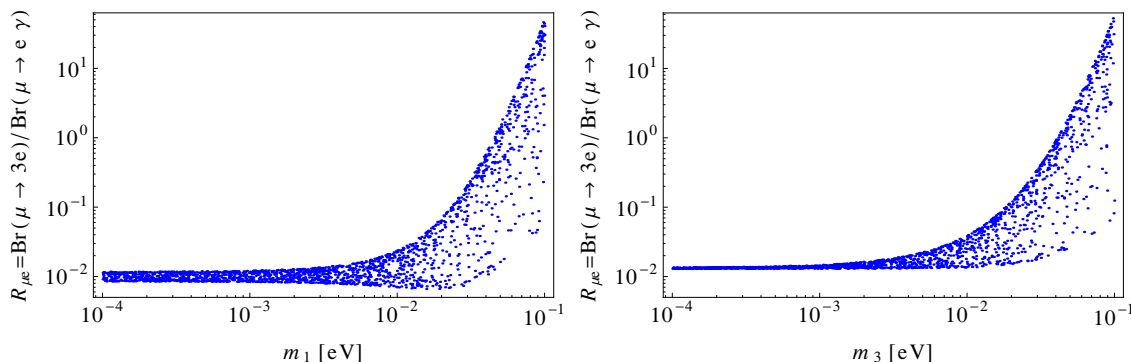


Figure 10. The ratio $R_{\mu e} = \text{Br}(\mu \rightarrow 3e)/\text{Br}(\mu \rightarrow e\gamma)$ as a function of the lightest neutrino mass. Scenario B is assumed, see text for details. To the left for NH, whereas to the right for IH.

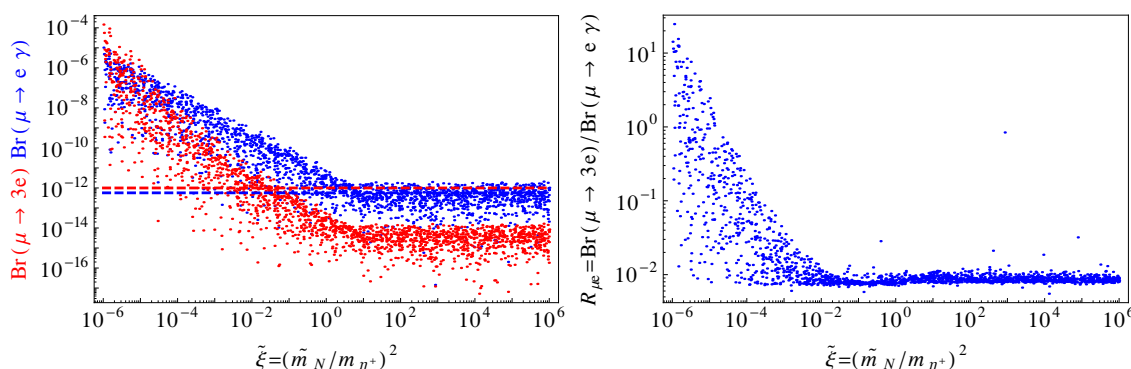


Figure 11. $\text{Br}(\mu \rightarrow e\gamma)$ and $\text{Br}(\mu \rightarrow 3e)$ (to the left) and the resulting $R_{\mu e}$ ratio (to the right) as a function of $\tilde{\xi} = (\tilde{m}_N/m_{\eta^+})^2$. Normal hierarchy for the light neutrinos and a non-degenerate right-handed neutrino spectrum (with $\tilde{m}_N^{(1)} = 2 \text{ TeV}$ and $\tilde{m}_N^{(2)} = 3 \text{ TeV}$) have been assumed, see text for details. The horizontal dashed lines show the current upper bounds.

Figure 11 shows a representative example of how the LFV rates can change in a non-degenerate right-handed neutrino spectrum. On the left, we show $\text{Br}(\mu \rightarrow e\gamma)$ (blue) and $\text{Br}(\mu \rightarrow 3e)$ (red) as a function of $\tilde{\xi} = (\tilde{m}_N/m_{\eta^+})^2$, where the horizontal dashed lines represent the current upper bounds on the branching ratios. On the right we show the resulting $R_{\mu e}$ ratio. Fixed values $\tilde{m}_N^{(1)} = 2 \text{ TeV}$, $\tilde{m}_N^{(2)} = 3 \text{ TeV}$, $m_{\eta^+} = 1 \text{ TeV}$ and $m_{\nu_1} = 10^{-3} \text{ eV}$ were assumed. A NH spectrum for the light neutrinos was chosen for this figure and we allowed for a random Dirac phase δ .

As naively expected, low \tilde{m}_N values enhance both branching ratios, with $\text{Br}(\mu \rightarrow 3e)$ being the one that typically gets the larger enhancements. This is caused by the large box contributions induced by the lightest right-handed neutrino. On the other hand, when $\tilde{m}_N \gg \tilde{m}_N^{(1,2)}$, the contribution of the heaviest right-handed neutrino (with a mass \tilde{m}_N) becomes sub-dominant and the LFV rates remain barely the same as in the degenerate case. This implies that the general conclusions drawn from the numerical results shown in this section are not restricted to degenerate scenarios. Besides this fact, we do not find any other remarkable feature in the LFV phenomenology for non-degenerate right-handed neutrinos.

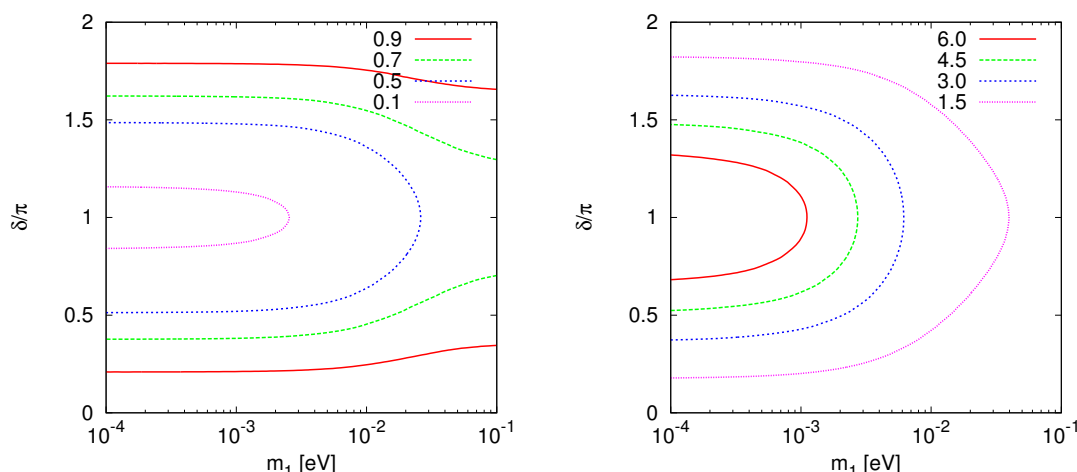


Figure 12. $\text{Br}(\ell_\alpha \rightarrow \ell_\beta \gamma) / \text{Br}(\ell_\alpha \rightarrow \ell_\beta \gamma)_{\delta=0}$ contours in the $m_{\nu_1} - \delta$ plane. To the left for $\ell_\alpha = \mu$ and $\ell_\beta = e$, to the right for $\ell_\alpha = \tau$ and $\ell_\beta = e$. Normal hierarchy for the light neutrinos, a degenerate right-handed neutrino spectrum and specific (but generic) values for the free parameters have been assumed, see text for more details.

4.2 Sensitivity to low-energy neutrino parameters

We have already shown the relevant role played by the lightest neutrino mass in the resulting LFV branching ratios. Let us now extend the discussion to the other undetermined low-energy parameter (besides the Majorana phases), the Dirac phase δ .

As starting point, we discuss how a non-zero Dirac phase can change the prediction for $\text{Br}(\ell_\alpha \rightarrow \ell_\beta \gamma)$. In order to do that, we consider the ratio $\text{Br}(\ell_\alpha \rightarrow \ell_\beta \gamma) / \text{Br}(\ell_\alpha \rightarrow \ell_\beta \gamma)_{\delta=0}$, where $\text{Br}(\ell_\alpha \rightarrow \ell_\beta \gamma)_{\delta=0}$ is the value of the branching ratio for $\delta = 0$. This is explicitly shown in figure 12, where contours of these ratios are drawn in the $m_{\nu_1} - \delta$ plane. In this figure we chose normal hierarchy for the light neutrinos, a degenerate right-handed neutrino spectrum and a real R matrix. Although these results were obtained for specific values of the remaining parameters, we emphasize that the $\text{Br}(\ell_\alpha \rightarrow \ell_\beta \gamma) / \text{Br}(\ell_\alpha \rightarrow \ell_\beta \gamma)_{\delta=0}$ does not depend on them when the right-handed neutrinos are degenerate and R is a real matrix, see eqs. (4.5) and (4.7).

The largest variations are found for $\text{Br}(\mu \rightarrow e \gamma)$ and $\text{Br}(\tau \rightarrow e \gamma)$, most directly affected by δ . For the former, we find that the branching ratio can be reduced by almost an order of magnitude, depending on the value of δ . In the latter case, the branching ratio can be increased by a factor of 4 just by switching on the Dirac phase. Moreover, in both cases we find that m_{ν_1} is also determinant. We do not show our results for the remaining case, $\ell_\alpha = \tau$ and $\ell_\beta = \mu$, since we found very little dependence on the Dirac phase.

These results tell us that the LFV rates are highly sensitive to the low-energy neutrino parameters. The question then arises as to whether one can get information about them by measuring LFV observables. In case of $\text{Br}(\ell_\alpha \rightarrow \ell_\beta \gamma)$, we have already seen that, for the specific scenario of degenerate right-handed neutrinos and a real R matrix, the flavor dependence of the amplitude will be determined just by low energy parameters: neutrino masses, mixing angles and CP violating phases. Therefore, by taking ratios of branching

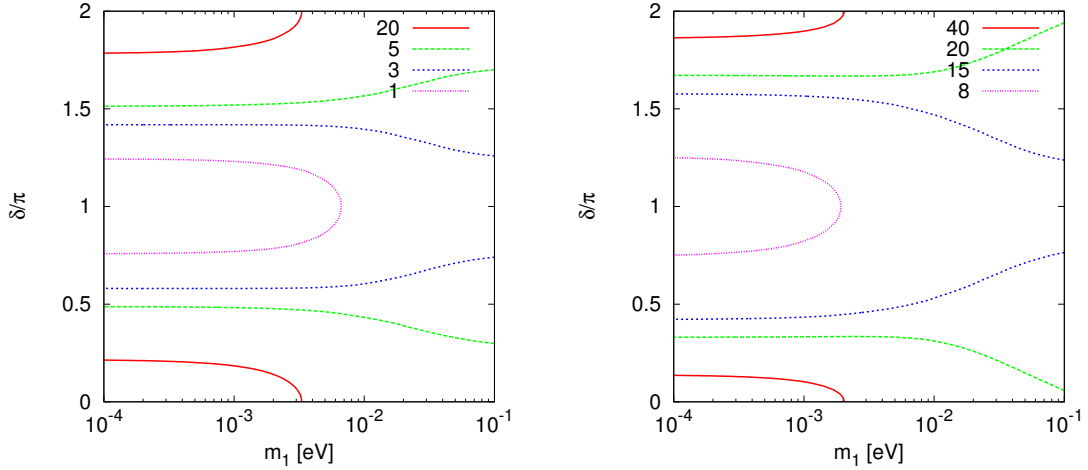


Figure 13. $\text{Br}(\ell_\alpha \rightarrow \ell_\beta \gamma) / \text{Br}(\ell_{\alpha'} \rightarrow \ell_{\beta'} \gamma)$ contours in the $m_{\nu_1} - \delta$ plane. To the left for $\ell_\alpha = \mu$, $\ell_{\alpha'} = \tau$ and $\ell_\beta = \ell_{\beta'} = e$, to the right for $\ell_\alpha = \ell_{\alpha'} = \tau$, $\ell_\beta = \mu$ and $\ell_{\beta'} = e$. Normal hierarchy for the light neutrinos, a degenerate right-handed neutrino spectrum and specific (but generic) values for the free parameters have been assumed, see text for more details.

ratios (what we call *flavor ratios*), the dependence on the high-energy parameters cancels out and we are left with functions of m_{ν_1} and δ . More precisely, we can make use of eqs. (4.5) and (4.7) to write

$$\frac{\text{Br}(\ell_\alpha \rightarrow \ell_\beta \gamma)}{\text{Br}(\ell_{\alpha'} \rightarrow \ell_{\beta'} \gamma)} = \frac{\left| \left(U_{\text{PMNS}} \hat{m}_\nu U_{\text{PMNS}}^\dagger \right)_{\beta\alpha} \right|^2}{\left| \left(U_{\text{PMNS}} \hat{m}_\nu U_{\text{PMNS}}^\dagger \right)_{\beta'\alpha'} \right|^2} \frac{\text{Br}(\ell_\alpha \rightarrow \ell_\beta \nu_\alpha \bar{\nu}_\beta)}{\text{Br}(\ell_{\alpha'} \rightarrow \ell_{\beta'} \nu_{\alpha'} \bar{\nu}_{\beta'})}. \quad (4.9)$$

Note that there is no sum over α , α' , β and β' in the previous expression.

Our results for these ratios are presented in figure 13. We show $\text{Br}(\mu \rightarrow e \gamma) / \text{Br}(\tau \rightarrow e \gamma)$ (to the left) and $\text{Br}(\tau \rightarrow \mu \gamma) / \text{Br}(\tau \rightarrow e \gamma)$ (to the right) contours in the $m_{\nu_1} - \delta$ plane. Under the assumptions of a degenerate right-handed neutrino spectrum and vanishing phases in the R matrix, this figure would allow one to set important constraints on m_{ν_1} and δ in case two branching ratios were measured. Furthermore, we see again the important dependence on these two low-energy parameters, since the ratios can change by more than one order of magnitude.

The same will be true for $\text{Br}(\ell_\alpha \rightarrow 3 \ell_\beta)$ when one of the two pieces, D_1 or D_2 , dominates. A particularly interesting scenario arises when the term containing the loop function $D_2 \subset B$ gives the dominant contribution. As we have found numerically, this assumption is typically valid for $\xi \gtrsim 10$ or for large m_{ν_1} . In this case, the special dependence on the Yukawa matrices, $(y^T y)_{\beta\beta} (y^T y)_{\beta\alpha}$, implies that the R matrix drops from the flavor ratios even when it contains complex entries, since $R^T R = 1$.

We have investigated this scenario and obtained the results in figure 14. We concentrate on $\text{Br}(\mu \rightarrow 3e) / \text{Br}(\tau \rightarrow 3e)$ (on the left) and $\text{Br}(\tau \rightarrow 3\mu) / \text{Br}(\tau \rightarrow 3e)$ (on the right). In the derivation of these plots, we neglected the contribution from the D_1 term. Moreover, we

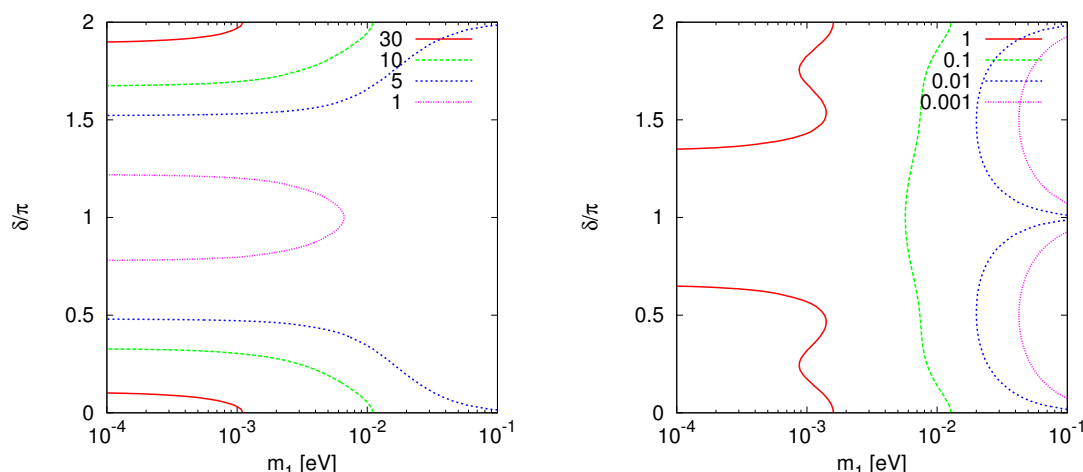


Figure 14. $\text{Br}(\ell_\alpha \rightarrow 3\ell_\beta)/\text{Br}(\ell_{\alpha'} \rightarrow 3\ell_{\beta'})$ contours in the $m_{\nu_1} - \delta$ plane. To the left for $\ell_\alpha = \mu$, $\ell_{\alpha'} = \tau$ and $\ell_\beta = \ell_{\beta'} = e$, to the right for $\ell_\alpha = \ell_{\alpha'} = \tau$, $\ell_\beta = \mu$ and $\ell_{\beta'} = e$. Normal hierarchy for the light neutrinos and a degenerate right-handed neutrino spectrum have been assumed, see text for more details.

assumed normal hierarchy for the light neutrinos and a degenerate right-handed neutrino spectrum. It is clear that, again, the parameters δ and m_{ν_1} may have a very strong impact on the 3-body branching ratios. On the left-hand side of the figure we see that (for this parameter configuration) $\text{Br}(\mu \rightarrow 3e)$ is typically larger than $\text{Br}(\tau \rightarrow 3e)$. The ratio between these two observables is only close to 1 for $\delta = \pi$, whereas in the rest of the $m_{\nu_1} - \delta$ plane one has $\text{Br}(\mu \rightarrow 3e) \gg \text{Br}(\tau \rightarrow 3e)$. On the other hand, the right-hand side of the figure shows that the ratio $\text{Br}(\tau \rightarrow 3\mu)/\text{Br}(\tau \rightarrow 3e)$ is mostly determined by m_{ν_1} , with δ playing a secondary role. As for the previous case, the ratio could be close to 1 (for low m_{ν_1}) or much larger (for high values of the lightest neutrino mass).

Our study reveals that LFV observables in the scotogenic model are highly sensitive to low-energy parameters such as the Dirac phase or the lightest neutrino mass. However, it also reveals a large degeneracy, this is, the LFV rates are not correlated with a single parameter. Furthermore, our results regarding flavor ratios have been obtained for a special case: degenerate right-handed neutrinos and real R matrix. In a more general scenario one expects departures from the values of the flavor ratios obtained here. In conclusion, it is not possible to determine the value of a single parameter by measuring a flavor ratio. Only the combination of measurements of the low-energy parameters with the discovery of one (or several) LFV processes can really put the flavor structure of the scotogenic model under experimental test.

4.3 $\mu - e$ conversion in nuclei

So far we have discussed our results on $\ell_\alpha \rightarrow \ell_\beta \gamma$ and $\ell_\alpha \rightarrow 3\ell_\beta$. Now we move on to discuss $\mu - e$ conversion in nuclei. In this model, we have found that Z -penguins give a very little contribution to $\mu - e$ conversion in nuclei compared to that of the γ -penguins. In

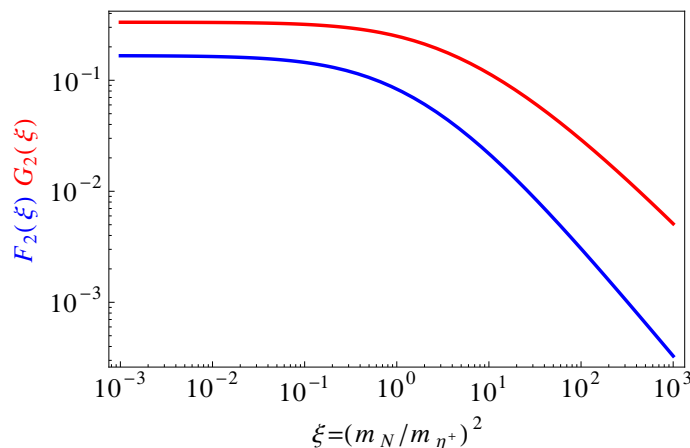


Figure 15. The loop functions $F_2(\xi)$ and $G_2(\xi)$ as a function of $\xi = (m_N/m_{\eta^+})^2$. For the definitions see appendix A.

this situation one could naively expect dipole operators to dominate the conversion rate. When this is the case, one expects a simple relation [53]

$$\frac{\text{CR}(\mu - e, \text{Nucleus})}{\text{Br}(\mu \rightarrow e\gamma)} \approx \frac{f(Z, N)}{428} \quad (4.10)$$

where $f(Z, N)$ is a function that depends on the nucleus and ranges from 1.1 to 2.2 for the nuclei of interest. However, in addition to the dipole contribution given by A_D , γ -penguins also have the non-dipole contribution given by A_{ND} . In fact, eqs. (3.2) and (3.5) tell us that, for degenerate right-handed neutrinos, one has $A_D = 3 F_2(\xi)/G_2(\xi) A_{ND}$. Therefore, the relative weight of these two different photon contributions depends on the loop functions $F_2(\xi)$ and $G_2(\xi)$. These are shown in figure 15, where one can see that $G_2(\xi) > F_2(\xi)$. For $\xi \ll 1$ the difference between $G_2(\xi)$ and $F_2(\xi)$ is small and both contributions have similar weights. However, for $\xi \gg 1$ ($m_N \gg m_{\eta^+}$) one has $G_2(\xi) \gg F_2(\xi)$ and A_{ND} becomes the most relevant contribution.⁹ This is illustrated in figure 16, where we show our results for $\text{Br}(\mu \rightarrow e\gamma)$ and $\text{CR}(\mu - e, \text{Ti})$, as well as their ratio. The same parameter configuration as in figure 6 has been selected: fixed values $m_{\eta^+} = 1 \text{ TeV}$ and $m_{\nu_1} = 10^{-3} \text{ eV}$, random real R matrix and Dirac phase. These numerical results were obtained for NH, although very similar results are found for IH. We focused on $\mu - e$ conversion in titanium, although the same behavior is found for other nuclei.

We find that for large values of ξ , the $\mu - e$ conversion rate in titanium gets enhanced by photonic non-dipole contributions. This is a positive result, given the great experimental perspectives for $\mu - e$ conversion in nuclei in the near future.

⁹Notice that we do not find the same behavior in $\text{Br}(\ell_\alpha \rightarrow 3 \ell_\beta)$ due to the additional (large) logarithmic factor that multiplies $|A_D|^2$ in the branching ratio formula, see eq. (3.11). Moreover, even if the photonic non-dipole terms can be slightly larger than the dipole ones, box diagrams give even larger contributions in the same region of parameter space.

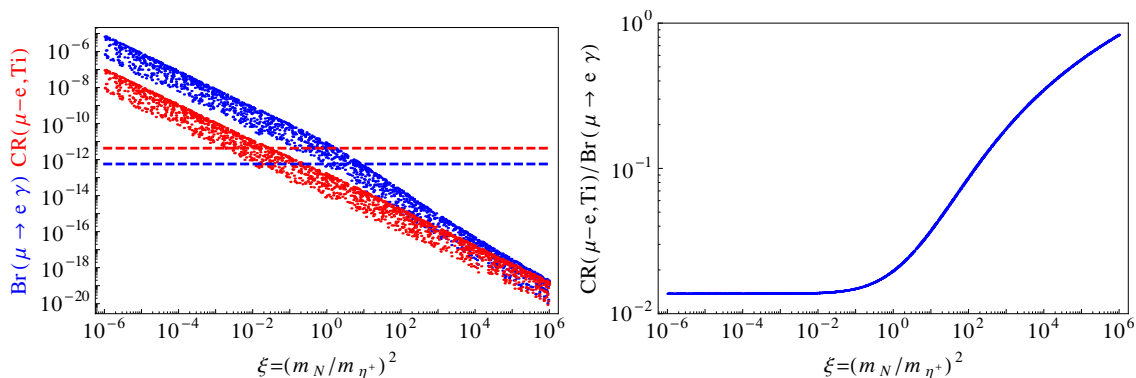


Figure 16. $\text{Br}(\mu \rightarrow e\gamma)$ and $\text{CR}(\mu - e, \text{Ti})$ (to the left) and the ratio $\text{CR}(\mu - e, \text{Ti})/\text{Br}(\mu \rightarrow e\gamma)$ (to the right) as a function of $\xi = (m_N/m_{\eta^+})^2$. Normal hierarchy for the light neutrinos and a degenerate right-handed neutrino spectrum have been assumed, see text for details. The horizontal dashed lines show the current upper bounds.

5 Summary and conclusions

The scotogenic model is a popular extension of the standard model that accounts for neutrino masses and dark matter. As for most neutrino mass models, lepton flavor violation is one of the most attractive phenomenological issues, as it may reveal the underlying mechanism that leads to neutrino masses and mixings. In this work we have studied the predictions obtained in the scotogenic model for the LFV processes with the best experimental perspectives in the near future: $\ell_\alpha \rightarrow \ell_\beta \gamma$, $\ell_\alpha \rightarrow 3\ell_\beta$ and $\mu - e$ conversion in nuclei. Full analytical expressions have been derived, going beyond the usual dipole dominance approximation. Our computation includes, besides the dipole photon penguin contribution, non-dipole photon contributions, Z -penguins as well as box diagrams.

The full consideration of all contributions to LFV processes leads to a very interesting picture. Given the rich LFV phenomenology in the scotogenic model, we are sure that more complete studies can be performed. Here we have explored some of the phenomenological consequences of our analytical results. This may serve as a summary of our main conclusions:

- Box diagrams dominate the LFV amplitudes in some parts of parameter space. This scenario leads to a deviation from the naive expectations obtained from the dipole dominance assumption and makes $\ell_\alpha \rightarrow 3\ell_\beta$ more constraining than $\ell_\alpha \rightarrow \ell_\beta \gamma$.
- The mass hierarchy between the right-handed neutrinos and the inert doublet scalars is of fundamental relevance for LFV observables. We have found that parameter points with large Yukawa couplings and $m_N \gg m_{\eta^+}$ or $m_N \ll m_{\eta^+}$ typically have enhanced box diagrams, thus leading to $\text{Br}(\ell_\alpha \rightarrow 3\ell_\beta) > \text{Br}(\ell_\alpha \rightarrow \ell_\beta \gamma)$. This is caused by the particular behavior of the loop functions.
- In the scotogenic model, there are two dark matter candidates: the lightest right-handed neutrino N_1 and the lightest neutral η scalar (η_R or η_I) [17]. When $\xi > 1$,

the lightest neutral η constitutes the dark matter of the universe. Otherwise, N_1 is the dark matter particle [29–31, 52]. In case of N_1 DM ($\xi < 1$), the only possible annihilation channel is $N_1 N_1 \rightarrow \ell_\alpha \bar{\ell}_\beta$, via the Yukawa interaction. For this reason, Yukawa couplings of $\mathcal{O}(1)$ are required in order to obtain the observed dark matter relic density $\Omega h^2 \approx 0.12$ [54], and this may lead to incompatibility with the LFV bounds. It is thus clear that the dark matter phenomenology of N_1 and LFV are closely related. We have explicitly constructed parameter points where all the requirements for right-handed neutrino dark matter are met: $m_N < m_\eta$, large Yukawa couplings and m_N in the appropriate range, as found in dedicated studies [52]. Our investigation reveals that although most of these points lead to violation of the LFV bounds, a small fraction of them are perfectly compatible. These valid points involve some small tuning of the parameters and could only be found due to the generality of our scans (not limited to any fixed structure of the Yukawa couplings). These results can be seen as a positive indication in favor of the validity of right-handed neutrino dark matter, although detailed studies are required to get a definitive and robust conclusion. These are, however, beyond the scope of this paper. On the other hand, we would like to point out that in case the dark matter is provided by the scalar η , one can always obtain the correct relic density since, in addition to the Yukawa interactions, this particle has gauge and scalar interactions [55, 56], not correlated with LFV.

- The LFV rates are highly sensitive to the low-energy parameters m_{ν_1} (the mass of the lightest neutrino) and δ (the Dirac phase). In particular, large m_{ν_1} typically enhances box diagrams.
- In some specific scenarios (with degenerate right-handed neutrinos), the ratios of branching ratios depend only on m_{ν_1} and δ . Under some assumptions, this may allow us to test the flavor structure of the model.
- Interestingly, the rate for $\mu - e$ conversion in nuclei can also be enhanced beyond the dipole contribution in some regions of the parameter space. Our study reveals that non-dipole photon contributions become very relevant for $m_N \gg m_{\eta^+}$. This may lead to $\mu - e$ conversion rates in nuclei as large as the branching ratio for $\mu \rightarrow e\gamma$. These are good news given the promising experimental projects in $\mu - e$ conversion in nuclei.

We would like to stress that our (qualitative) conclusions are not restricted to Ma’s scotogenic model, but should apply to a much wider class of radiative neutrino mass models. In particular, extended versions of the scotogenic model (like the model proposed in [57]) should have, at least in some corners of parameter space, a similar phenomenology.

The presence of TeV scale particles with sizable couplings to the SM states also leads to interesting prospects at the LHC. Although the direct production of the right-handed neutrinos is typically suppressed due to their singlet nature, they will be produced in the decays of the η scalars when this is kinematically allowed. In turn, the η scalars may

have non-negligible production cross-sections provided they are light. This possibility, not related to the lepton sector, has been studied in some detail. In this case one expects multilepton final states with a significant amount of missing energy [58]. Furthermore, the scotogenic states may also modify the usual Higgs boson decays, with observable implications at the LHC [59, 60].

To conclude, the anatomy of lepton flavor violation in the scotogenic model has been fully determined and some interesting phenomenological aspects have been explored. Some definite predictions have been made, and these may be used to put the model under experimental test. The connection between neutrino masses and lepton flavor violation is a powerful test for this purpose. Hopefully, a positive signal in one (or several) experiments in the next few years will provide valuable hints on the mechanism behind neutrino masses.

Acknowledgments

We would like to thank Thomas Schwetz for many fruitful discussions. AV also thanks Nuria Rius and Juan Racker for their comments on the manuscript and acknowledges partial support from the ANR project CPV-LFV-LHC NT09-508531. TT acknowledges support from the European ITN project (FP7-PEOPLE-2011-ITN, PITN-GA-2011-289442-INVISIBLES).

A Loop functions

We present in this appendix the loop functions that appear in the paper,

$$F_2(x) = \frac{1 - 6x + 3x^2 + 2x^3 - 6x^2 \log x}{6(1-x)^4}, \quad (\text{A.1})$$

$$G_2(x) = \frac{2 - 9x + 18x^2 - 11x^3 + 6x^3 \log x}{6(1-x)^4}, \quad (\text{A.2})$$

$$D_1(x, y) = -\frac{1}{(1-x)(1-y)} - \frac{x^2 \log x}{(1-x)^2(x-y)} - \frac{y^2 \log y}{(1-y)^2(y-x)}, \quad (\text{A.3})$$

$$D_2(x, y) = -\frac{1}{(1-x)(1-y)} - \frac{x \log x}{(1-x)^2(x-y)} - \frac{y \log y}{(1-y)^2(y-x)}. \quad (\text{A.4})$$

These loop functions do not have any poles. In the limit $x, y \rightarrow 1$ and $y \rightarrow x$, the functions become

$$F_2(1) = \frac{1}{12}, \quad G_2(1) = \frac{1}{4}, \quad D_1(1, 1) = -\frac{1}{3}, \quad D_2(1, 1) = \frac{1}{6}, \quad (\text{A.5})$$

$$D_1(x, x) = \frac{-1 + x^2 - 2x \log x}{(1-x)^3}, \quad (\text{A.6})$$

$$D_1(x, 1) = D_1(1, x) = \frac{-1 + 4x - 3x^2 + 2x^2 \log x}{2(1-x)^3}, \quad (\text{A.7})$$

$$D_2(x, x) = \frac{-2 + 2x - (1+x) \log x}{(1-x)^3}, \quad (\text{A.8})$$

$$D_2(x, 1) = D_2(1, x) = \frac{1 - x^2 + 2x \log x}{2(1-x)^3}. \quad (\text{A.9})$$

B Flavor structures

Using the conventions in eq. (2.10) and neglecting the Majorana phases one finds

- $U_{\text{PMNS}} \hat{m}_\nu U_{\text{PMNS}}^\dagger$

$$\left(U_{\text{PMNS}} \hat{m}_\nu U_{\text{PMNS}}^\dagger \right)_{11} = c_{13}^2 (c_{12}^2 m_1 + m_2 s_{12}^2) + m_3 s_{13}^2, \quad (\text{B.1})$$

$$\left(U_{\text{PMNS}} \hat{m}_\nu U_{\text{PMNS}}^\dagger \right)_{22} = s_{23}^2 [s_{13}^2 (c_{12}^2 m_1 + m_2 s_{12}^2) + c_{13}^2 m_3] + c_{23}^2 (c_{12}^2 m_2 + m_1 s_{12}^2) \quad (\text{B.2})$$

$$+ 2 c_{12} c_{23} s_{12} s_{13} s_{23} \cos \delta (m_1 - m_2),$$

$$\left(U_{\text{PMNS}} \hat{m}_\nu U_{\text{PMNS}}^\dagger \right)_{33} = c_{23}^2 [s_{13}^2 (c_{12}^2 m_1 + m_2 s_{12}^2) + c_{13}^2 m_3] + s_{23}^2 (c_{12}^2 m_2 + m_1 s_{12}^2) \quad (\text{B.3})$$

$$+ 2 c_{12} c_{23} s_{12} s_{13} s_{23} \cos \delta (m_2 - m_1),$$

$$\left(U_{\text{PMNS}} \hat{m}_\nu U_{\text{PMNS}}^\dagger \right)_{21} = c_{12} c_{13} s_{12} c_{23} (m_2 - m_1) + c_{13} s_{13} s_{23} e^{-i\delta} [m_3 - m_2 + c_{12}^2 (m_2 - m_1)], \quad (\text{B.4})$$

$$\left(U_{\text{PMNS}} \hat{m}_\nu U_{\text{PMNS}}^\dagger \right)_{31} = c_{12} c_{13} s_{12} s_{23} (m_1 - m_2) + c_{13} s_{13} c_{23} e^{-i\delta} [m_3 - m_2 + c_{12}^2 (m_2 - m_1)], \quad (\text{B.5})$$

$$\left(U_{\text{PMNS}} \hat{m}_\nu U_{\text{PMNS}}^\dagger \right)_{32} = c_{23} s_{23} [(s_{12}^2 - c_{12}^2 s_{13}^2) (m_2 - m_1) + c_{13}^2 (m_3 - m_2)] \quad (\text{B.6})$$

$$- c_{12} s_{12} s_{13} (c_{23}^2 e^{i\delta} - s_{23}^2 e^{-i\delta}) (m_2 - m_1).$$

- $U_{\text{PMNS}}^* \hat{m}_\nu U_{\text{PMNS}}^\dagger$

$$\left(U_{\text{PMNS}}^* \hat{m}_\nu U_{\text{PMNS}}^\dagger \right)_{11} = c_{13}^2 (c_{12}^2 m_1 + m_2 s_{12}^2) + e^{-2i\delta} m_3 s_{13}^2, \quad (\text{B.7})$$

$$\left(U_{\text{PMNS}}^* \hat{m}_\nu U_{\text{PMNS}}^\dagger \right)_{22} = s_{23}^2 [e^{2i\delta} s_{13}^2 (c_{12}^2 m_1 + m_2 s_{12}^2) + c_{13}^2 m_3] + c_{23}^2 (c_{12}^2 m_2 + m_1 s_{12}^2) \quad (\text{B.8})$$

$$+ 2 c_{12} c_{23} s_{12} s_{13} s_{23} e^{i\delta} (m_1 - m_2),$$

$$\left(U_{\text{PMNS}}^* \hat{m}_\nu U_{\text{PMNS}}^\dagger \right)_{33} = c_{23}^2 [e^{2i\delta} s_{13}^2 (c_{12}^2 m_1 + m_2 s_{12}^2) + c_{13}^2 m_3] + s_{23}^2 (c_{12}^2 m_2 + m_1 s_{12}^2) \quad (\text{B.9})$$

$$+ 2 c_{12} c_{23} s_{12} s_{13} s_{23} e^{i\delta} (m_2 - m_1),$$

$$\left(U_{\text{PMNS}}^* \hat{m}_\nu U_{\text{PMNS}}^\dagger \right)_{21} = c_{12} c_{13} s_{12} c_{23} (m_2 - m_1) + c_{13} s_{13} s_{23} e^{i\delta} [e^{-2i\delta} m_3 - m_2 + c_{12}^2 (m_2 - m_1)], \quad (\text{B.10})$$

$$\left(U_{\text{PMNS}}^* \hat{m}_\nu U_{\text{PMNS}}^\dagger \right)_{31} = c_{12} c_{13} s_{12} s_{23} (m_1 - m_2) + c_{13} s_{13} c_{23} e^{i\delta} [e^{-2i\delta} m_3 - m_2 + c_{12}^2 (m_2 - m_1)], \quad (\text{B.11})$$

$$\left(U_{\text{PMNS}}^* \hat{m}_\nu U_{\text{PMNS}}^\dagger \right)_{32} = c_{23} s_{23} [(s_{12}^2 - e^{2i\delta} c_{12}^2 s_{13}^2) (m_2 - m_1) + c_{13}^2 (m_3 - e^{2i\delta} m_2) + (e^{2i\delta} - 1) m_2], \quad (\text{B.12})$$

$$- c_{12} s_{12} s_{13} e^{i\delta} (c_{23}^2 - s_{23}^2) (m_2 - m_1).$$

Open Access. This article is distributed under the terms of the Creative Commons Attribution License ([CC-BY 4.0](https://creativecommons.org/licenses/by/4.0/)), which permits any use, distribution and reproduction in any medium, provided the original author(s) and source are credited.

References

- [1] MEG collaboration, J. Adam et al., *New limit on the lepton-flavour violating decay $\mu^+ \rightarrow e^+ \gamma$* , *Phys. Rev. Lett.* **107** (2011) 171801 [[arXiv:1107.5547](#)] [[INSPIRE](#)].
- [2] MEG collaboration, J. Adam et al., *New constraint on the existence of the $\mu^+ \rightarrow e^+ \gamma$ decay*, *Phys. Rev. Lett.* **110** (2013) 201801 [[arXiv:1303.0754](#)] [[INSPIRE](#)].
- [3] A. Baldini et al., *MEG Upgrade Proposal*, [arXiv:1301.7225](#) [[INSPIRE](#)].
- [4] A. Blondel et al., *Research Proposal for an Experiment to Search for the Decay $\mu \rightarrow eee$* , [arXiv:1301.6113](#) [[INSPIRE](#)].
- [5] MU2E collaboration, D. Glenzinski, *The Mu2e Experiment at Fermilab*, *AIP Conf. Proc.* **1222** (2010) 383 [[INSPIRE](#)].
- [6] MU2E collaboration, R.M. Carey et al., *Proposal to search for $\mu^- N \rightarrow e^- N$ with a single event sensitivity below 10^{-16}* , [FERMILAB-PROPOSAL-0973](#).
- [7] DEEME collaboration, M. Aoki, *A new idea for an experimental search for μ -e conversion*, [PoS\(ICHEP 2010\)279](#).
- [8] COMET collaboration, Y.G. Cui et al., *Conceptual design report for experimental search for lepton flavor violating $\mu^- \rightarrow e^-$ conversion at sensitivity of 10^{-16} with a slow-extracted bunched proton beam*, KEK-2009-10 [[INSPIRE](#)].
- [9] PRIME Working Group, *Search for the $\mu \rightarrow e$ Conversion Process at an Ultimate Sensitivity of the Order of 10^{-18} with PRISM*, LOI to J-PARC 50-GeV PS, LOI-25, unpublised http://j-parc.jp/researcher/Hadron/en/pac_0606/pdf/p20-Kuno.pdf.
- [10] SUPERB collaboration, B. O'Leary et al., *SuperB Progress Reports — Physics*, [arXiv:1008.1541](#) [[INSPIRE](#)].
- [11] BELLE, BELLE II collaborations, K. Hayasaka, *Results and prospects on lepton flavor violation at Belle/Belle II*, *J. Phys. Conf. Ser.* **408** (2013) 012069 [[INSPIRE](#)].
- [12] BABAR collaboration, B. Aubert et al., *Searches for Lepton Flavor Violation in the Decays $\tau^\pm \rightarrow e^\pm \gamma$ and $\tau^\pm \rightarrow \mu^\pm \gamma$* , *Phys. Rev. Lett.* **104** (2010) 021802 [[arXiv:0908.2381](#)] [[INSPIRE](#)].
- [13] SINDRUM collaboration, U. Bellgardt et al., *Search for the Decay $\mu^+ \rightarrow e^+ e^+ e^-$* , *Nucl. Phys. B* **299** (1988) 1 [[INSPIRE](#)].
- [14] K. Hayasaka et al., *Search for Lepton Flavor Violating τ Decays into Three Leptons with 719 Million Produced $\tau^+ \tau^-$ Pairs*, *Phys. Lett. B* **687** (2010) 139 [[arXiv:1001.3221](#)] [[INSPIRE](#)].
- [15] SINDRUM II collaboration, W.H. Bertl et al., *A search for muon to electron conversion in muonic gold*, *Eur. Phys. J. C* **47** (2006) 337 [[INSPIRE](#)].
- [16] SINDRUM II collaboration, C. Dohmen et al., *Test of lepton flavor conservation in $\mu \rightarrow e$ conversion on titanium*, *Phys. Lett. B* **317** (1993) 631 [[INSPIRE](#)].
- [17] E. Ma, *Verifiable radiative seesaw mechanism of neutrino mass and dark matter*, *Phys. Rev. D* **73** (2006) 077301 [[hep-ph/0601225](#)] [[INSPIRE](#)].
- [18] H. Okada and T. Toma, *Fermionic Dark Matter in Radiative Inverse Seesaw Model with $U(1)_{B-L}$* , *Phys. Rev. D* **86** (2012) 033011 [[arXiv:1207.0864](#)] [[INSPIRE](#)].
- [19] P.B. Dev and A. Pilaftsis, *Minimal Radiative Neutrino Mass Mechanism for Inverse Seesaw Models*, *Phys. Rev. D* **86** (2012) 113001 [[arXiv:1209.4051](#)] [[INSPIRE](#)].

- [20] M. Aoki, J. Kubo and H. Takano, *Two-loop radiative seesaw with multicomponent dark matter explaining the possible gamma excess in the Higgs boson decay and at the Fermi LAT*, *Phys. Rev. D* **87** (2013) 116001 [[arXiv:1302.3936](#)] [[INSPIRE](#)].
- [21] Y. Kajiyama, H. Okada and T. Toma, *Multicomponent dark matter particles in a two-loop neutrino model*, *Phys. Rev. D* **88** (2013) 015029 [[arXiv:1303.7356](#)] [[INSPIRE](#)].
- [22] S. Kanemura, T. Matsui and H. Sugiyama, *Loop Suppression of Dirac Neutrino Mass in the Neutrinophilic Two Higgs Doublet Model*, *Phys. Lett. B* **727** (2013) 151 [[arXiv:1305.4521](#)] [[INSPIRE](#)].
- [23] S.S. Law and K.L. McDonald, *A Class of Inert N-tuplet Models with Radiative Neutrino Mass and Dark Matter*, *JHEP* **09** (2013) 092 [[arXiv:1305.6467](#)] [[INSPIRE](#)].
- [24] M. Hirsch, R. Lineros, S. Morisi, J. Palacio, N. Rojas and J.W.F. Valle, *WIMP dark matter as radiative neutrino mass messenger*, *JHEP* **10** (2013) 149 [[arXiv:1307.8134](#)] [[INSPIRE](#)].
- [25] D. Restrepo, O. Zapata and C.E. Yaguna, *Models with radiative neutrino masses and viable dark matter candidates*, *JHEP* **11** (2013) 011 [[arXiv:1308.3655](#)] [[INSPIRE](#)].
- [26] E. Ma, I. Picek and B. Radovčić, *New Scotogenic Model of Neutrino Mass with $U(1)_D$ Gauge Interaction*, *Phys. Lett. B* **726** (2013) 744 [[arXiv:1308.5313](#)] [[INSPIRE](#)].
- [27] M. Lindner, D. Schmidt and A. Watanabe, *Dark matter and $U(1)'$ symmetry for the right-handed neutrinos*, [arXiv:1310.6582](#) [[INSPIRE](#)].
- [28] H. Okada and K. Yagyu, *Radiative Generation of the Lepton Mass*, [arXiv:1311.4360](#) [[INSPIRE](#)].
- [29] J. Kubo, E. Ma and D. Suematsu, *Cold Dark Matter, Radiative Neutrino Mass, $\mu \rightarrow e\gamma$ and Neutrinoless Double Beta Decay*, *Phys. Lett. B* **642** (2006) 18 [[hep-ph/0604114](#)] [[INSPIRE](#)].
- [30] D. Aristizabal Sierra, J. Kubo, D. Restrepo, D. Suematsu and O. Zapata, *Radiative seesaw: Warm dark matter, collider and lepton flavour violating signals*, *Phys. Rev. D* **79** (2009) 013011 [[arXiv:0808.3340](#)] [[INSPIRE](#)].
- [31] D. Suematsu, T. Toma and T. Yoshida, *Reconciliation of CDM abundance and $\mu \rightarrow e\gamma$ in a radiative seesaw model*, *Phys. Rev. D* **79** (2009) 093004 [[arXiv:0903.0287](#)] [[INSPIRE](#)].
- [32] A. Adulpravitchai, M. Lindner and A. Merle, *Confronting Flavour Symmetries and extended Scalar Sectors with Lepton Flavour Violation Bounds*, *Phys. Rev. D* **80** (2009) 055031 [[arXiv:0907.2147](#)] [[INSPIRE](#)].
- [33] J. Casas and A. Ibarra, *Oscillating neutrinos and $\mu \rightarrow e, \gamma$* , *Nucl. Phys. B* **618** (2001) 171 [[hep-ph/0103065](#)] [[INSPIRE](#)].
- [34] A. Ilakovac and A. Pilaftsis, *Flavor violating charged lepton decays in seesaw-type models*, *Nucl. Phys. B* **437** (1995) 491 [[hep-ph/9403398](#)] [[INSPIRE](#)].
- [35] F. Deppisch and J. Valle, *Enhanced lepton flavor violation in the supersymmetric inverse seesaw model*, *Phys. Rev. D* **72** (2005) 036001 [[hep-ph/0406040](#)] [[INSPIRE](#)].
- [36] F. Deppisch, T. Kosmas and J. Valle, *Enhanced $\mu^- \rightarrow e^-$ conversion in nuclei in the inverse seesaw model*, *Nucl. Phys. B* **752** (2006) 80 [[hep-ph/0512360](#)] [[INSPIRE](#)].
- [37] A. Ilakovac and A. Pilaftsis, *Supersymmetric Lepton Flavour Violation in Low-Scale Seesaw Models*, *Phys. Rev. D* **80** (2009) 091902 [[arXiv:0904.2381](#)] [[INSPIRE](#)].
- [38] R. Alonso, M. Dhen, M. Gavela and T. Hambye, *Muon conversion to electron in nuclei in type-I seesaw models*, *JHEP* **01** (2013) 118 [[arXiv:1209.2679](#)] [[INSPIRE](#)].

- [39] D. Dinh, A. Ibarra, E. Molinaro and S. Petcov, *The $\mu - e$ Conversion in Nuclei, $\mu \rightarrow e\gamma$, $\mu \rightarrow 3e$ Decays and TeV Scale See-Saw Scenarios of Neutrino Mass Generation*, *JHEP* **08** (2012) 125 [Erratum *ibid.* **1309** (2013) 023] [[arXiv:1205.4671](#)] [[INSPIRE](#)].
- [40] A. Ilakovac, A. Pilaftsis and L. Popov, *Charged lepton flavor violation in supersymmetric low-scale seesaw models*, *Phys. Rev. D* **87** (2013) 053014 [[arXiv:1212.5939](#)] [[INSPIRE](#)].
- [41] A. Abada, D. Das, A. Vicente and C. Weiland, *Enhancing lepton flavour violation in the supersymmetric inverse seesaw beyond the dipole contribution*, *JHEP* **09** (2012) 015 [[arXiv:1206.6497](#)] [[INSPIRE](#)].
- [42] P.S.B. Dev, C.-H. Lee and R. Mohapatra, *Natural TeV-Scale Left-Right Seesaw for Neutrinos and Experimental Tests*, *Phys. Rev. D* **88** (2013) 093010 [[arXiv:1309.0774](#)] [[INSPIRE](#)].
- [43] E. Arganda and M.J. Herrero, *Testing supersymmetry with lepton flavor violating tau and mu decays*, *Phys. Rev. D* **73** (2006) 055003 [[hep-ph/0510405](#)] [[INSPIRE](#)].
- [44] J. Hisano, T. Moroi, K. Tobe and M. Yamaguchi, *Lepton flavor violation via right-handed neutrino Yukawa couplings in supersymmetric standard model*, *Phys. Rev. D* **53** (1996) 2442 [[hep-ph/9510309](#)] [[INSPIRE](#)].
- [45] Y. Kuno and Y. Okada, *Muon decay and physics beyond the standard model*, *Rev. Mod. Phys.* **73** (2001) 151 [[hep-ph/9909265](#)] [[INSPIRE](#)].
- [46] E. Arganda, M. Herrero and A. Teixeira, *$\mu - e$ conversion in nuclei within the CMSSM seesaw: Universality versus non-universality*, *JHEP* **10** (2007) 104 [[arXiv:0707.2955](#)] [[INSPIRE](#)].
- [47] H. Chiang, E. Oset, T. Kosmas, A. Faessler and J. Vergados, *Coherent and incoherent (μ^- , e^-) conversion in nuclei*, *Nucl. Phys. A* **559** (1993) 526 [[INSPIRE](#)].
- [48] T. Kosmas, S. Kovalenko and I. Schmidt, *Nuclear $\mu^- - e^-$ conversion in strange quark sea*, *Phys. Lett. B* **511** (2001) 203 [[hep-ph/0102101](#)] [[INSPIRE](#)].
- [49] M. Gonzalez-Garcia, M. Maltoni, J. Salvado and T. Schwetz, *Global fit to three neutrino mixing: critical look at present precision*, *JHEP* **12** (2012) 123 [[arXiv:1209.3023](#)] [[INSPIRE](#)].
- [50] D. Forero, M. Tortola and J. Valle, *Global status of neutrino oscillation parameters after Neutrino-2012*, *Phys. Rev. D* **86** (2012) 073012 [[arXiv:1205.4018](#)] [[INSPIRE](#)].
- [51] G. Fogli, E. Lisi, A. Marrone, D. Montanino, A. Palazzo and A.M. Rotunno, *Global analysis of neutrino masses, mixings and phases: entering the era of leptonic CP-violation searches*, *Phys. Rev. D* **86** (2012) 013012 [[arXiv:1205.5254](#)] [[INSPIRE](#)].
- [52] D. Schmidt, T. Schwetz and T. Toma, *Direct Detection of Leptophilic Dark Matter in a Model with Radiative Neutrino Masses*, *Phys. Rev. D* **85** (2012) 073009 [[arXiv:1201.0906](#)] [[INSPIRE](#)].
- [53] INTENSITY FRONTIER CHARGED LEPTON WORKING GROUP collaboration, J. Albrecht et al., *Charged Leptons*, [arXiv:1311.5278](#) [[INSPIRE](#)].
- [54] PLANCK collaboration, P. Ade et al., *Planck 2013 results. XVI. Cosmological parameters*, [arXiv:1303.5076](#) [[INSPIRE](#)].
- [55] S. Kashiwase and D. Suematsu, *Baryon number asymmetry and dark matter in the neutrino mass model with an inert doublet*, *Phys. Rev. D* **86** (2012) 053001 [[arXiv:1207.2594](#)] [[INSPIRE](#)].

- [56] S. Kashiwase and D. Suematsu, *Leptogenesis and dark matter detection in a TeV scale neutrino mass model with inverted mass hierarchy*, *Eur. Phys. J. C* **73** (2013) 2484 [[arXiv:1301.2087](#)] [[INSPIRE](#)].
- [57] Y. Farzan, *A minimal model linking two great mysteries: neutrino mass and dark matter*, *Phys. Rev. D* **80** (2009) 073009 [[arXiv:0908.3729](#)] [[INSPIRE](#)].
- [58] M. Gustafsson, S. Rydbeck, L. Lopez-Honorez and E. Lundstrom, *Status of the Inert Doublet Model and the Role of multileptons at the LHC*, *Phys. Rev. D* **86** (2012) 075019 [[arXiv:1206.6316](#)] [[INSPIRE](#)].
- [59] S.-Y. Ho and J. Tandean, *Probing Scotogenic Effects in Higgs Boson Decays*, *Phys. Rev. D* **87** (2013) 095015 [[arXiv:1303.5700](#)] [[INSPIRE](#)].
- [60] A. Arhrib, Y.-L.S. Tsai, Q. Yuan and T.-C. Yuan, *An Updated Analysis of Inert Higgs Doublet Model in light of the Recent Results from LUX, PLANCK, AMS-02 and LHC*, [arXiv:1310.0358](#) [[INSPIRE](#)].